Remote Sensing Applications: Society and Environment 41 (2026) 101838

Contents lists available at ScienceDirect

Remote Sensing Applications: Society and Environment

journal homepage: www.elsevier.com/locate/rsase

Where rivers sleep: mapping ephemeral sand rivers in the West African Sahel

Axel Belemtougri [a,*], Roland Yonaba [b], Claire I. Michailovsky [c], Tibor Stigter [c], Lawani Adjadi Mounirou [b], Pieter van der Zaag [c,d]

[a] Département Gestion des Ressources Naturelles et Systèmes de Productions, Institut de l'Environnement et de Recherches Agricoles (INERA), 04 BP 8645, Ouagadougou, Burkina Faso
[b] Laboratoire Eaux, Hydro-Systèmes et Agriculture (LEHSA), Institut International d'Ingénierie de l'Eau et de l'Environnement (2iE), 01 BP 594, Ouagadougou, Burkina Faso
[c] IHE Delft Institute for Water Education, P.O. Box 3015, 2601, DA, Delft, the Netherlands
[d] Department of Water Management, Delft University of Technology, P.O. Box 5048, 2600, DA, Delft, the Netherlands

ARTICLE INFO

Keywords:
Ephemeral sand rivers
Remote sensing
Riparian vegetation
Sentinel-2
West Africa

ABSTRACT

This study presents a new geospatial framework for detecting and mapping ephemeral sand rivers (ESRs) across the West African Sahel, focusing on Burkina Faso, Mali, and Niger, where food security challenges are acute. ESRs, which remain dry most of the year, act as vital subsurface water reservoirs in arid environments. During the wet season, infiltrated streamflow is stored within sandy beds, minimizing evaporative losses and providing shallow groundwater with potential to support domestic, livestock, and agricultural needs during dry periods. The methodology integrates hydrological analyses, remote sensing, and machine learning. A high-resolution drainage network was derived from the 90 m MERIT DEM, based on national reference river networks and satellite-derived information. A Random Forest model predicted river flow intermittency and identified ephemeral rivers (flowing 1–4 months annually, catchment area $\geq$1000 km^2), around which 500 m buffer zones were delineated for analysis. Two composite thresholds (CTs) combining NDESI–NDVI spectral indices achieved moderate accuracy: CT1 (42 %) and CT2 (72 %), with CT2 serving as a first-order tool for sandy riverbed detection. A multi-temporal supervised land use/land cover classification achieved high accuracy (92 %) and F1 scores >0.86, outperforming the spectral thresholds. Using vegetation presence as a proxy for shallow groundwater, 19 % of ESRs (402 km) were identified as areas of potentially accessible water storage near settlements representing about 3 million people (4.8 % of the population) across the three countries. These findings highlight the importance of ESRs for sustainable water management and climate-resilient livelihoods in the Sahel.

1. Introduction

Non-perennial rivers (NPRs) represent a substantial component of global river networks, especially in arid and semi-arid regions where they serve as a crucial yet often overlooked water resource. Characterized by intermittent or ephemeral flow regimes, NPRs encompass a spectrum of hydrological behaviors, from intermittent rivers that experience predictable, seasonal flow cessation, to

* Corresponding author. Ouagadougou 06, 06-BP-9115, Burkina Faso.
E-mail address: axelbelemtougri@gmail.com (A. Belemtougri).

https://doi.org/10.1016/j.rsase.2025.101838
Received 20 October 2025; Received in revised form 11 December 2025; Accepted 11 December 2025
Available online 12 December 2025

ephemeral rivers that flow only in direct response to rainfall events (Belemtougri et al., 2021b; Costigan et al., 2017; Fovet et al., 2021; Goodrich et al., 2018). While NPRs are present across all continents, they are particularly dominant in Africa. Recent studies estimate that approximately 71 % of the total river length on the continent experiences at least one month (i.e., 30 days) of zero flow per year (Messager et al., 2021). Despite their variable hydrological nature, these rivers provide essential ecological functions and contribute significantly to local livelihoods by facilitating groundwater recharge and acting as temporary water reservoirs.

A specific and highly valuable subset of NPRs is the ephemeral sand river (ESR), which plays a vital role in dryland hydrology, particularly across the Sahelian zone. These rivers are typically defined by their broad sandy beds, ranging at depths between 2 and 20 m, with high infiltration capacity. This geomorphological structure allows them to function as natural alluvial aquifers, capturing and storing alluvial water beneath the surface (Herbert et al., 1997; Morin et al., 2009; Saveca et al., 2022a; Shanafield and Cook, 2014). Unlike surface water bodies that are prone to high evaporation rates (Codjia et al., 2025; Girard et al., 2025; Lèye et al., 2021), ESRs can retain water underground, ensuring year-round availability for smallholder agriculture, livestock, and domestic use (Villeneuve et al., 2015; Walker et al., 2019). Recharge generally occurs through episodic flood events during the rainy season, enabling the formation of shallow aquifers that persist well into the dry season (Kafando et al., 2021, 2022; Rau et al., 2017). Given increasing water scarcity across dryland regions, these ESRs represent a renewable and easily accessible water resource with high potential to support rural livelihoods in terms of domestic use, livestock and agriculture (Ryan and Elsner, 2016; Vio et al., 2025).

The West African Sahel (WAS) is currently facing acute water stress, driven by a combination of demographic growth and climate change (Donat et al., 2016; Fowé et al., 2023; Nkiaka et al., 2024). By 2045, the region's population is projected to increase by approximately 140 million, resulting in surging demand for freshwater resources (United Nations, 2022). Simultaneously, climate projections forecast significant warming, up to +3 °C by 2050 and + 4.3 °C by 2080, alongside increasing rainfall variability and more frequent extreme droughts (Niang et al., 2014; O'Gorman, 2015; Panthou et al., 2014; Todzo et al., 2020). These changes pose serious threats to regional food security, as agriculture remains largely rain-fed and highly sensitive to climate variability. In this context, improved identification and sustainable utilization of ESRs could provide a critical buffer against water deficits, facilitating resilient agricultural practices and reducing dependency on erratic rainfall (Sanogo et al., 2024).

Despite their strategic importance, ESRs remain poorly documented in the WAS, particularly in comparison to Eastern and Southern Africa where their hydrology and socio-economic relevance have been more thoroughly investigated (Duker et al., 2020; Love et al., 2011; Mansell and Hussey, 2005; Saveca et al., 2022; Svubure et al., 2011; Thirumalraj et al., 2023; Walker et al., 2019;

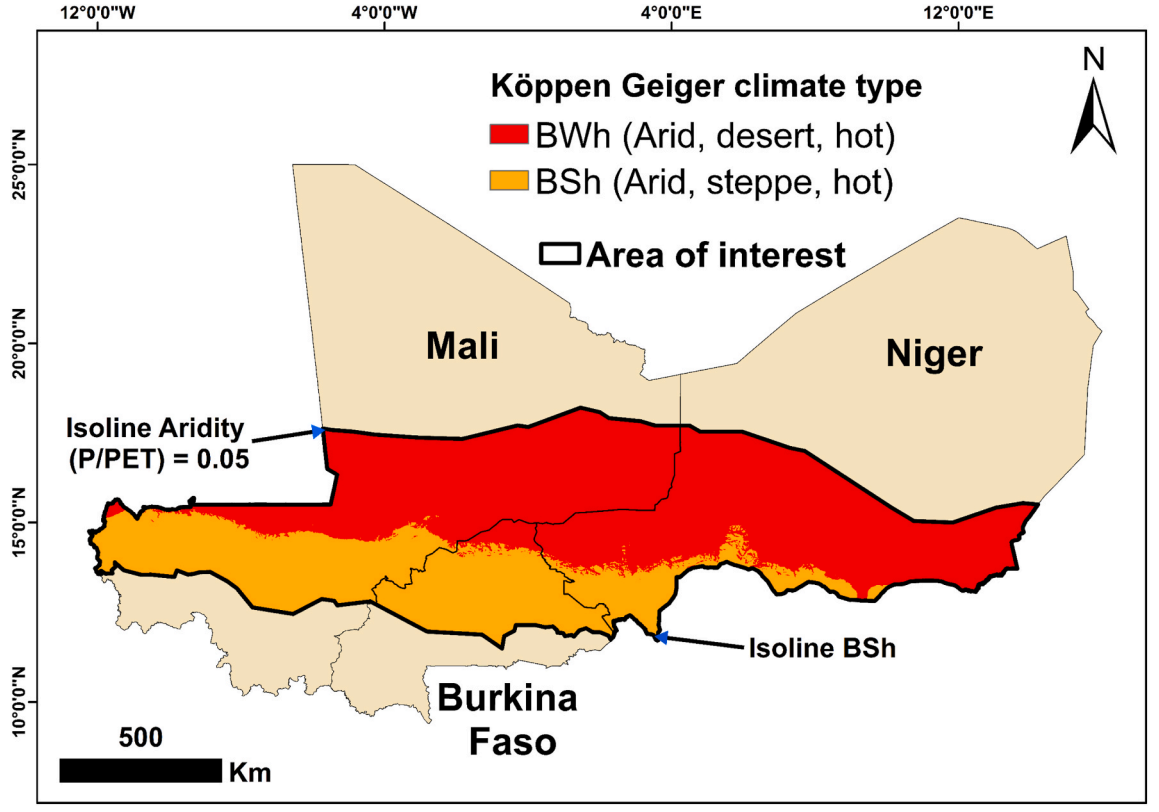

Fig. 1. The study area is delineated by an aridity index >0.05 and by the BSh and BWh climate types (Beck et al., 2018; Peel et al., 2007), ***in West African Sahel (Burkina Faso, Mali and Niger).*** *The aridity index isoline (P/ETP = 0.05) is the ratio between the average annual precipitation and the average annual potential evapotranspiration over the period 2014–2024 in the study area. Climate data are sourced from the CHIRPS dataset (*Funk et al., 2015*) at a resolution of 0.05° (approximately 5.5* km *at the equator).*

Wekesa et al., 2020). In these regions, farmer-led irrigation has successfully leveraged the latent water storage capacity of ESRs (Mpala et al., 2016; Wekesa et al., 2020). In contrast, the WAS suffers from a lack of systematic mapping, hydrological characterization, and policy integration concerning these vital systems. However, the recent advancements in earth observation technologies, geographic information systems (GIS), machine learning algorithms and cloud-computing platforms (Yonaba et al., 2025) offer new opportunities for the detection, classification, and assessment of ESRs at larger scale. Nonetheless, these tools must be carefully adapted to the unique environmental characteristics of the WAS, including sandy substrates, sparse vegetation, and marked seasonal hydrological variability.

This study aims to develop a robust methodological framework for the systematic detection and mapping of ephemeral sand rivers (ESRs) in Burkina Faso, Mali, and Niger, using an integrated approach based on combining remote sensing, GIS, and machine learning. The specific objectives of the study are: (1) to evaluate the utility of optical remote sensing satellite data for identifying optimal spectral indices suited to distinguishing sandy riverbeds from surrounding land use/land cover (LULC); (2) to develop an integrated supervised classification to differentiate ESRs from other LULC types; and (3) to leverage the presence of perennial riparian vegetation and canopy height as an indicator of shallow groundwater availability. By producing the first large-scale ESR inventory for the West African Sahel, this research seeks to inform water resource planning, support climate change adaptation strategies, and contribute to farmer-led irrigation development. Ultimately, the findings may enhance regional food security and promote sustainable agricultural livelihoods in one of the most water-vulnerable regions of the world.

2. Materials and methods

2.1. Study area description

This study focuses on Burkina Faso, Mali, and Niger, three landlocked countries located in West Africa (Fig. 1). These countries exhibit substantial climatic variability, particularly regarding rainfall distribution and the duration of the wet season. Precipitation displays a pronounced spatial gradient, ranging from less than 100 mm/yr in the hyper-arid northern regions of Mali and Niger to approximately 1200 mm/yr in the more humid southern regions of Burkina Faso (Nicholson, 2013; PNA, 2015; Yonaba et al., 2024). Similarly, the wet season varies in length, extending from less than two months in the northern arid zones to up to five months in the southern, semi-humid areas (Dembélé et Zwart, 2016; Jalloh et al., 2013; Yonaba et al., 2024).

A distinct climatic gradient characterizes the study area, with increasing annual precipitation, a greater number of rainy months, and decreasing potential evapotranspiration rates from north to south. The northern parts of Mali and Niger are predominantly classified as desert climates (BWh) according to the Köppen–Geiger classification, while the southern parts of Burkina Faso and Mali fall within the tropical savanna climate zone (Aw) (Le Houérou, 2009; Peel et al., 2007). A large portion of the study area lies within the Sahelian belt, a transitional, arid to semi-arid zone extending from northern Senegal to Djibouti, which is characterized by a prolonged dry season lasting eight to nine months followed by a short-wet season of three to four months (Kardjadj, 2019). Precipitation in this zone typically ranges from 100 to 400 mm per year, underscoring the region's chronic water scarcity and heightened vulnerability to climate variability and extremes (Biasutti, 2019; Giannini et al., 2008).

Land use/land cover (LULC) across Burkina Faso, Mali, and Niger is largely shaped by agro-pastoral activities, with extensive livestock rearing and subsistence farming dominating rural economies, particularly within the Sahelian zones (Lèye et al., 2021; Mortimore et al., 2009; Nori and Davies, 2007; Yonaba et al., 2021). Rainfed agriculture remains the primary mode of food production, though it is highly susceptible to climatic shocks due to erratic rainfall patterns and the widespread lack of irrigation infrastructure (Kaboré et al., 2024; Sultan and Gaetani, 2016). Population density is generally low in the northern arid areas but increases markedly toward the south, especially near major water bodies and in areas suitable for seasonal agriculture (United Nations, 2022). Urbanization remains relatively limited to national capitals and a few secondary cities, with the majority of the population residing in rural areas and depending heavily on natural water sources for their livelihoods.

In this context, ESRs play a particularly important role. By providing seasonal water storage in otherwise dry environments, ESRs support smallholder agriculture, livestock watering, and domestic use. The proximity of rural populations to ESRs is thus of critical interest in this study. Specifically, this research will assess the distribution of ESRs in relation to population settlement patterns, highlighting the potential for ESR-based water resource development.

2.2. Geographical delineation of the study focus

To ensure the relevance of the analysis to semi-arid river systems, this study excludes regions classified as hyper-arid, defined by a precipitation-to-potential evapotranspiration ratio (P/PET) or aridity index of less than 0.05 according to the UNEP guidelines (Boschetto et al., 2010). This threshold ensures the removal of areas with extremely limited rainfall and negligible hydrological activity, such as the northern most zones of Mali and Niger.

To further refine the focus on rivers with hydrological significance over the past decade (2014–2024), an additional criterion was applied: only areas with at least one rainy month per year, defined as a month with cumulative precipitation exceeding 30 mm (corresponding to an average daily threshold >1 mm) to be considered a rainy day (Froidurot and Diedhiou, 2017), were retained. Moreover, to ensure hydrological persistence and the potential for regular aquifer recharge, the study includes only those areas where at least 90 % of the years within the period (2014–2024) recorded a minimum of one rainy month, see **Supplementary Material (SM)** Figs. S1–S2. This ensures the inclusion of rivers that experience at least one flow event in nine out of ten years, thus supporting the consistent replenishment of shallow alluvial aquifers, which is a key functional feature of ESRs, in particular when considering their potential for agricultural development (Walker et al., 2019).

Conversely, river systems located within more humid regions specifically those falling under the tropical savannah (*Aw*) climate classification, with average precipitation between 900 and 1200 mm/yr are also excluded. These areas, primarily located in southern Burkina Faso and Mali, are more conducive to off-season agriculture through conventional water sources and irrigation development, and therefore fall outside the scope of this study, which prioritizes the Sahelian semi-arid context (see **SM-**Fig. S3).

The overall methodology is summarized in Fig. 2. The methodological process begins with the extraction of the national river network and the prediction of river flow intermittency to identify ephemeral rivers (**SM** Fig. S4), around which a 250-m buffer zone is created (i.e., 500 m total buffer width, **SM** Fig. S5). Subsequently, Sentinel-2A images (2020–2024) are processed to remove clouds and shadows. A sand-characteristics spectral-based index and a multi-temporal supervised classification (Random Forest) are then applied to identify sandy riverbeds. Finally, groundwater access potential in alluvial aquifers was assessed.

2.3. *Mapping ephemeral rivers*

The accurate identification of ESRs depends on the careful delineation of the river network within the study area (**Step 1-** Fig. 2, **SM** Fig. S6). In this study, national reference river networks were used for the countries under investigation when available, given their superior accuracy compared to available global river datasets (Belemtougri et al., 2021a; Marešová et al., 2024). For Burkina Faso and Mali, the river networks were sourced from their respective national geographic institutes. However, due to limited access to institutional data in Niger, an enhanced river network dataset derived from remote-sensing data was used as an alternative (Wortmann et al., 2025). This approach emphasized the use of locally validated geospatial information to reduce the uncertainties associated with broader-scale datasets. A detailed description of the river network sources and their characteristics is presented in Table 1.

To enable detailed geospatial analysis of river reaches and their associated catchments, as well as a more precise characterization of flow regimes, the collected reference river networks were integrated into a digital elevation model (DEM). This integration facilitates the extraction of catchment characteristics at the river reach scale. To achieve this, the stream burning technique (Lindsay, 2016), was applied to embed the collected reference river networks into the Multi-Error-Removed Improved Terrain (MERIT) and Advanced World 3D (AW3D) DEMs at 90 m resolution (JAXA, 2019; Yamazaki et al., 2017, 2019). This resolution was selected as the optimal tradeoff between spatial detail and computational efficiency given the size of the total area to be processed.

Different upstream contributing area thresholds, between 1 km^2 and 2.5 km^2, were tested for river stream extraction. Visual assessment indicated that the MERIT DEM more accurately captured the spatial variability of river systems compared to the AW3D

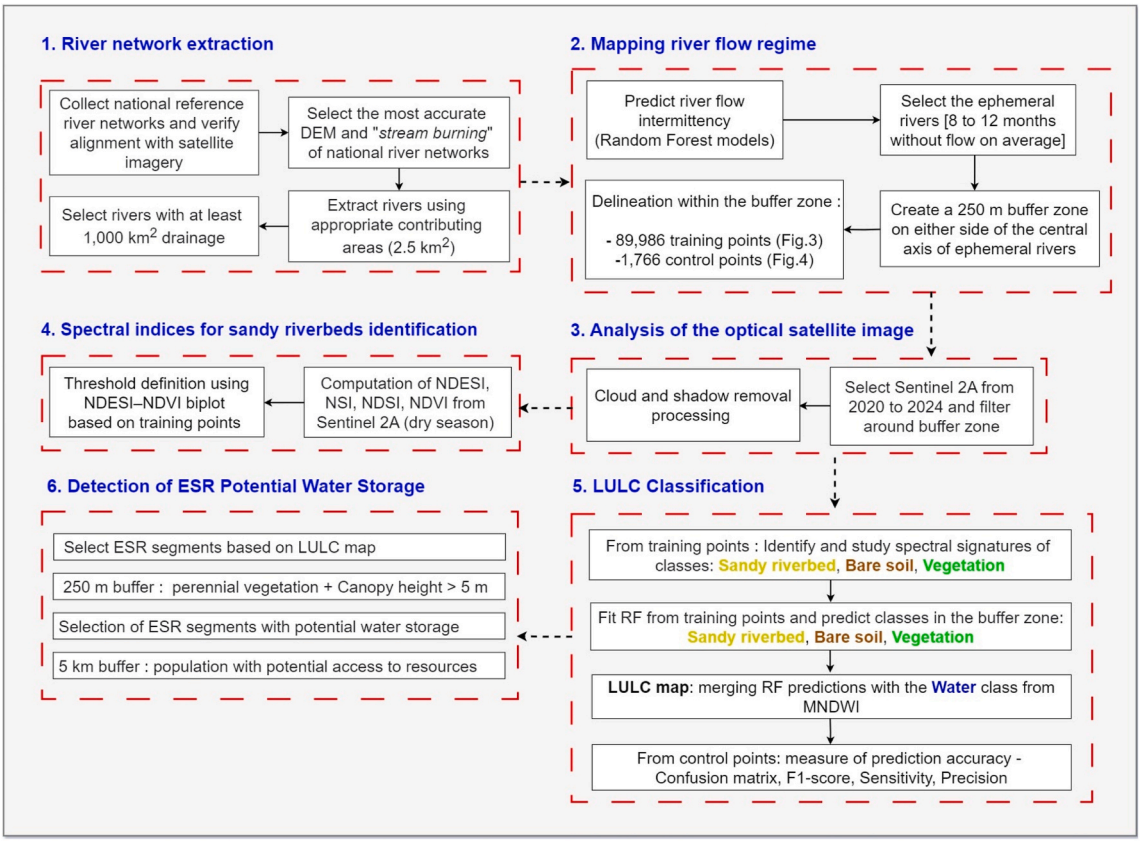

Fig. 2. Flowchart of the methodological framework used in this study.

Table 1
Description of the reference river network in Burkina Faso, Mali, and Niger.

Country	Data source	Source imagery	Spatial resolution	Processing method
Burkina Faso	National Geographic Institute in Burkina Faso (IGB-Institut Géographique du Burkina, 2012)	RapidEye satellite images	5 m	Digitized river network from imagery
Mali	National Geographic Institute in Mali (IGM-Institut Géographique du Mali, 2016)	SPOT 6 satellite images	1.5 m	Digitized river network from imagery
Niger	Wortmann et al. (2025)	Landsat River mask (GRWL) + FABDEM DEM	30 m	Merged river data from GRWL and FABDEM DEM for accuracy improvement

DEM, leading to its selection for the rest of the analysis. Furthermore, the 2.5 km^2 threshold was found to provide a better representation of the observed river network structure, whereas the lower thresholds generated a higher number of false positives. Consequently, the 2.5 km^2 threshold was adopted for this study. Flow direction and flow accumulation grids derived from the MERIT DEM were ultimately used to delineate the catchments associated with each river reach within the selected river network (Linke et al., 2019).

To classify river flow regimes in the study area (**Step 2 –** Fig. 2), with a particular emphasis on ephemeral rivers, we rely on a sequential modeling approach using Random Forest classifiers and leverage spatially distributed hydro-environmental predictors (**SM** Table S1**, SM** Fig. S7) to estimate river flow regimes (Belemtougri et al., 2025a). To mitigate class imbalance in the training dataset (**SM** Table S2), the sequential Random Forest approach decomposes the prediction task into two models (Döll et al., 2024). First, a Binary Classification (BC) distinguishes perennial from non-perennial reaches, thereby reducing the influence of the majority class in dominating the learning process. A second multiclass model (MC) further categorizes non-perennial reaches as weakly intermittent, highly intermittent, or ephemeral, which effectively rebalances the training data and improves their classification performance. The models used were trained on flow data from 1269 gauging stations across the African continent, covering the period from 1958 to 1998 (**SM** Table S3). They employed the mean annual number of zero-flow months ($\overline{Ndry}$) as a key predictor to assign the gauges to one of four intermittency classes and demonstrated satisfactory predictive performance (BC: balanced accuracy = 0.81; MC: balanced accuracy = 0.68), where balanced accuracy is defined as the average of sensitivity (the proportion of correctly identified perennial gauges) and specificity (the proportion of correctly identified non-perennial gauges), providing a metric that remains reliable even when classes are imbalanced (see **SM** Table S4).

To account for the broad variability in flow patterns, four flow regime classes were defined based on increasing levels of intermittency: perennial (0–1 month of zero flow), weakly intermittent (2–4 months), highly intermittent (5–7 months), and ephemeral (8–12 months). This multi-class classification scheme offers a significant advantage over a binary classification (ephemeral vs. non-ephemeral), particularly in the context of an imbalanced training dataset where ephemeral rivers are underrepresented; while a binary approach (perennial vs non-perennial) would likely result in oversimplifying the continuum of intermittency and ignoring the environmental gradients that influence these transitions (Belemtougri et al., 2025a). The refined classification used here (four classes of flow intermittency) enables more accurate representation of the hydrological complexity observed at the regional scale (**SM** Fig. S4).

In this study, particular attention is given to the ephemeral class (8–12 months of zero flow annually, i.e. just 1–4 months of annual flow). These rivers exhibit the shortest flow duration compared to other intermittency classes, meaning that identifying potential shallow groundwater resources within these channels could have a particularly significant impact on the communities living nearby. To further refine the sample, we consider only those ephemeral rivers with a drainage area of at least 1000 km^2 (**SM** Fig. S5). This threshold helps exclude small ESRs where development for irrigation would likely represent conflicts with critical and competing water uses such as drinking water supply, sanitation, and livestock watering (Benjaminsen et al., 2021; Raynaut, 2001).

2.4. Remote sensing data and analyses

In this study, we used Maxar ground-truth high resolution satellite imagery within ESRI ArcGIS Pro (version 3.1.5) to generate training and validation points for the characterization of spectral indices and the implementation of a supervised classification approach (**Step 2 –** Fig. 2). The considered LULC classes are "*Bare soil*", "*Vegetation*", "*Water*" and "*Sandy riverbed*". A detailed description of these LULC categories is provided in Table 2.

Table 2
Description of the selected LULC categories in the study area.

LULC type	Description
Sandy riverbed	Ephemeral riverbeds composed primarily of light-colored, fine sand (typically white or pale beige), dry during the dry season and may function as subsurface aquifers for groundwater storage.
Bare soil	Exposed soil surfaces including uncultivated land, degraded lands, or sandy soils not associated with riverbeds. This class includes golden sands (sand dunes) and dry agricultural plots. Pavement, erosion or desiccation crusts developing at the soil surface. Includes roads, settlements, buildings, rooftops.
Vegetation	Areas with perennial vegetation, including trees, shrubs, and grasslands, cultures, found along riparian corridors or adjacent floodplains.
Water	Open surface water present within or adjacent to riverbeds (dams, lake, etc.), including stagnant pools, ponds, or slow-flowing sections of ephemeral rivers. Often greenish in imagery due to algae presence or ochre-colored due to high turbidity from suspended particles.

Training and validation points were generated within a 250 m buffer around the centerlines of the selected ephemeral rivers (each draining at least 1000 km^2). This buffer size was chosen to fully encompass the expected maximum channel width of these rivers. The analysis of GRIT width statistics (Wortmann et al., 2025) shows that rivers of this magnitude in the study area typically have median and average widths of 83 m and 160 m, respectively, well within the 250 m radial distance. Using this restricted buffer also helps maintain computational efficiency during supervised classification at 10 m resolution, while ensuring that all relevant riverbed pixels are included.

Training areas corresponding to different LULC types were delineated by digitizing polygons at multiple locations where these classes were clearly identifiable (313 in total), using LULC context offered by Maxar ground-truth high-resolution satellite imagery (0.3–0.5 m pixel resolution, 5 m geolocation accuracy) acquired in the dry season (Fig. 3).

These training areas were subsequently converted to points, accounting for the 10 m resolution, which yielded 89,986 spatially distributed training samples across the study area. To further reduce spatial autocorrelation between training and validation datasets, particularly in cases where points might originate from neighboring locations, validation points were generated independently using a spatially separate random sampling procedure that did not overlap with the training polygons (Fig. 4).

The LULC mapping method developed in this study was implemented within the Google Earth Engine (GEE) platform (Gorelick et al., 2017). The Sentinel-2A optical imagery, comprising 13 spectral bands (B1–B12 and B8A) at spatial resolutions of 10 m, 20 m, and 60 m, was employed for ESR detection (Drusch et al., 2012). On GEE, the S2_SR_HARMONIZED (Sentinel-2 Surface Reflectance Harmonized) product was used, offering atmospherically and radiometrically corrected imagery with more consistent surface reflectance values. To ensure uniformity across all computations, bands with native resolutions above 10 m were resampled to 10 m spatial resolution.

Cloud removal from Sentinel-2 Surface Reflectance (SR) data was carried out using the QA60 quality band (**Step 3 –** Fig. 2), which provides encoded information on cloud and shadow presence (Codjia et al., 2025; Li et al., 2024). Subsequent geospatial data processing was performed using ESRI ArcGIS Pro (version 3.1.5), based on outputs generated through Google Earth Engine (GEE).

The SR images collection period spans from 2020 to 2024, corresponding to the five most recent years for which consistent Sentinel-2 and Maxar ground-truth imagery are available. To account for seasonal LULC variations, which are highly typical of the Sahelian context (Yonaba et al., 2021), the SR images were reduced to median multitemporal images, stacking three distinct sub-periods in the year:

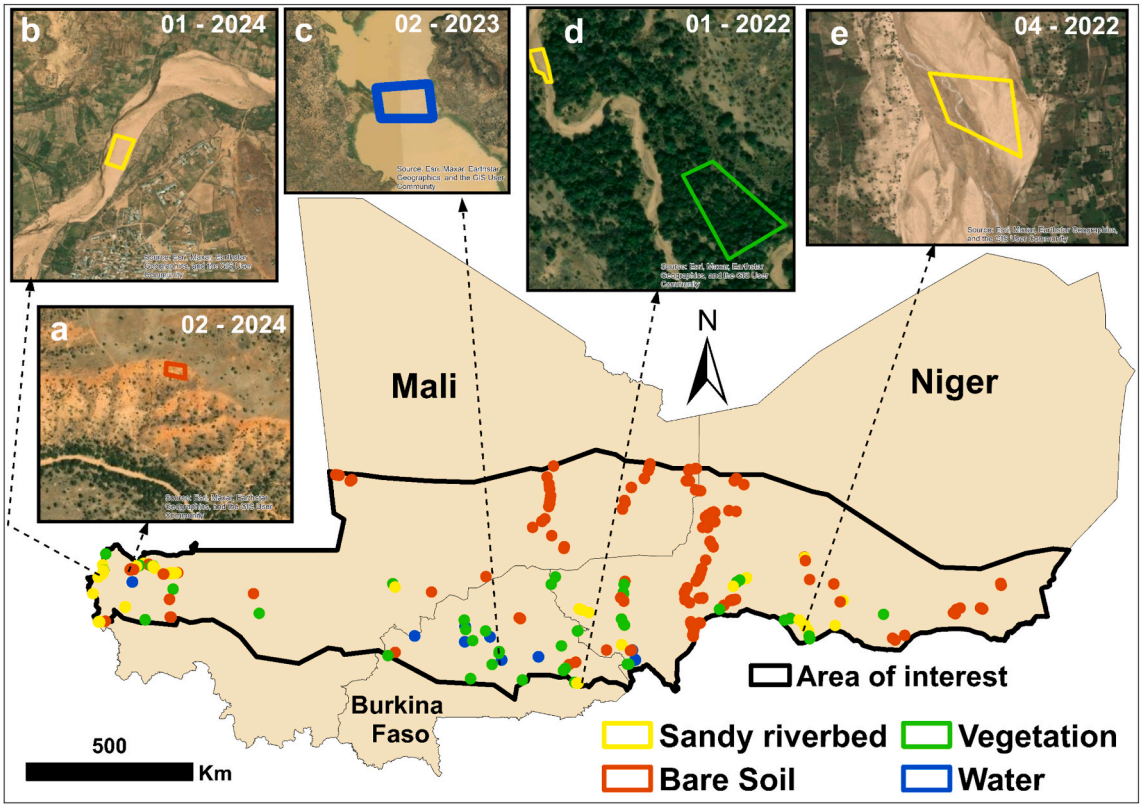

Fig. 3. Spatial distribution of training areas (313) in the study area. The processing of these training areas resulted in a total of 89,986 spatially distributed training points across the study area, classified as follows: Sandy riverbeds: 4317 points, Bare soil: 48,750 points, Vegetation: 4090 points and water: 32,829 points.

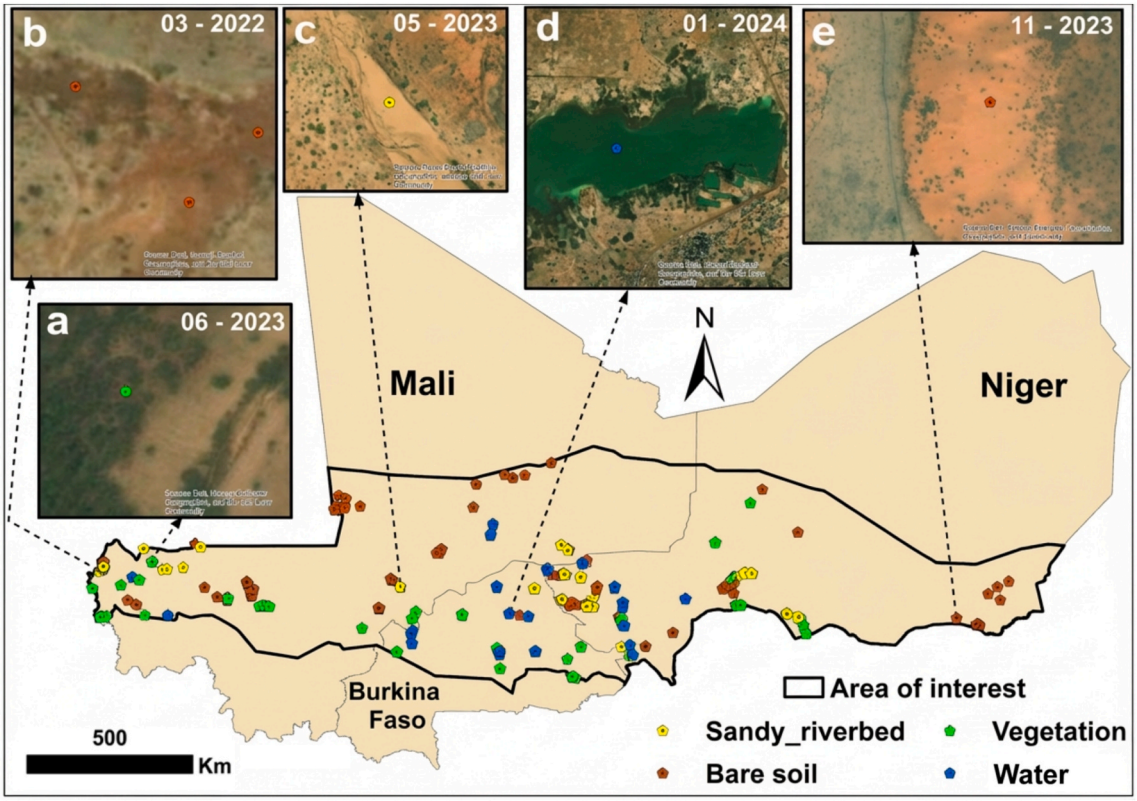

Fig. 4. Spatial distribution of validation points in the study area (1,766). Specifically, the classes contain the following samples: Sandy riverbed (351), Bare soil (388), Vegetation (506), Water (521).

- a dry period (February to May), marked by the absence of rainfall and peak annual temperatures;
- a wet period (June to September), corresponding to the rainy season, with relatively moderate temperatures;
- a transition period (October to January), defined by low or no precipitation and the lowest annual temperatures.

To address the first objective (**Step 4 –** Fig. 2), i.e. to identify satellite-derived spectral indices suitable for characterization of sandy riverbeds in the West African Sahel, a literature review was conducted, which led to the selection of a set of relevant indices (Table 3). For the purpose of index calculation, only the dry period was considered. This timing was selected based on the assumption that ESRs are most likely to be drier in this period of the year and therefore more readily detectable during periods of no precipitation.

All spectral index calculations were applied within the 250 m buffer surrounding the river network centerlines (see **SM** Fig. S5). In Google Earth Engine (GEE), surface reflectance values, typically expressed within the range of 0–1, are scaled by a factor of 10,000, by default. Accordingly, these values were rescaled to the [0–1] range prior to their use in the computation of the spectral indices presented in Table 3. For each selected index, median values were calculated over the dry season period from February 1, 2020, to May 31, 2024, using only cloud-free observations. The Normalized Sand Index (NSI) values were subsequently min–max normalized, resulting in a linear transformation of the data to the [0–1] scale, while preserving the relative distribution of the original values, as recommended by previous study (Secu et al., 2022). The distributions of spectral index values across the predefined LULC classes (Fig. 3) were analyzed to identify the index offering the highest discriminatory power for the "Sandy riverbed" class. Furthermore, the relationship between the selected sand-sensitive index and median NDVI (Normalized Difference Vegetation Index) values was

Table 3
Spectral indices used for mapping ephemeral sandy riverbeds.

Spectral indices definition	Formulas	Range/Sand threshold values	References
Normalized Difference Enhanced Sand Index (NDESI)	$NDESI = \frac{Red - Blue}{Red + Blue} - \frac{SWIR2 - SWIR1}{SWIR2 - SWIR1}$ (1)	[-2; 2]/> 0.24	(Marzouki and Dridri, 2022)
Normalized Sand Index (NSI)	$NSI = \frac{Green + Red}{log\,(SWIR1)}$ (2)	]-∞; 1]	Secu et al. (2022)
Normalized Difference Sand Index (NDSI)	$NDSI = \frac{Red - Coastal\ aerosol}{Red + Coastal\ aerosol}$ (3)	[-1; 1]	Pan et al. (2018)

examined to enhance differentiation among land cover types. NDVI was specifically used to discriminate vegetated surfaces, characterized by high near-infrared reflectance and strong red absorption due to chlorophyll, from non-vegetated surfaces such as dry sand and open water, which both exhibit low NDVI values. Coupling the sand-sensitive index with NDVI therefore allows effective separation of sandy riverbeds from vegetated riparian zones, while also reducing confusion between sand and water surfaces (Nkiaka et al., 2024). This dual-index approach supported the development of a composite threshold combining sand-specific and vegetation-related spectral indices, improving the automated detection of sandy riverbed pixels. The NDVI was calculated as shown in Equation (4):

$$NDVI = \frac{NIR - Red}{NIR + Red} \tag{4}$$

where *NIR* and *Red* are respectively the surface reflectance values in the *Near Infrared* and *Red* bands.

Composite thresholds were determined and subsequently applied to the sand-specific spectral index and the Normalized Difference Vegetation Index (NDVI) within the buffer to identify ESR areas. The spatial accuracy of the delineated ESRs zones was evaluated using the 351 validation points classified as sandy riverbed (Fig. 4). Given the extensive spatial coverage of the study area across three Sahelian countries (Burkina Faso, Mali and Niger), a case study site in Niger was selected as an illustrative example to visually assess the performance of the spectral indices in distinguishing sandy riverbeds from the surrounding landscape. This site was chosen for its clear representation of diverse land cover types, including ephemeral sandy riverbeds, sparse vegetation, bare soil and open water (**SM** Fig. S8). While this site serves as a visual illustration rather than an independent transfer test, the spectral thresholds and supervised classification were derived and validated using spatially distributed training and validation samples across the entire tri-national study domain, which already encompasses a wide range of Sahelian environmental conditions.

For the second objective of this study (**Step 5 –** Fig. 2), the supervised classification was used to map LULC types within the delineated buffer zone and was carried out using the Random Forest (RF) algorithm (Breiman, 2001), within the Google Earth Engine (GEE) platform. RF is a widely applied ensemble learning method in remote sensing due to its robustness, non-parametric formulation, and capacity to manage high-dimensional input data. The algorithm constructs multiple decision trees during training and aggregates their outputs to enhance classification accuracy while reducing overfitting (Boulesteix et al., 2012; Cutler et al., 2007). RF is frequently used in remote sensing for tasks such as land cover classification, change detection, and the estimation of biophysical variables from multispectral, hyperspectral, or LiDAR data (Belgiu and Drăguţ, 2016). Its effectiveness in handling noisy, heterogeneous data makes it particularly suitable for analyzing complex environmental systems (Tyralis et al., 2019).

The Random Forest (RF) model used in this study was run in classification mode with default hyperparameters: 500 decision trees (*ntree* = 500) and the number of variables randomly selected at each split set to $mtry = \sqrt{p}$, where p is the number of explanatory variables (Biau and Scornet, 2016). Preliminary hyperparameter tuning tests were conducted using alternative values of *ntree* and *mtry*; however, these tests did not yield any substantial improvement in classification accuracy or F1-scores. Given the very large spatial extent of the study area and the associated computational burden, default parameters were therefore retained as a computationally efficient and robust solution. This also indicates that classification performance is far more sensitive to the temporal structuring of the input data (multi-season composites) than to fine-scale RF hyperparameter tuning.

Three atmospheric bands (bands 1, 9, and 10) were excluded as they are mainly used for monitoring atmospheric conditions (Rossi et al., 2025), leaving out 10 useable bands. The explanatory dataset thereby formed consisted of 30 spectral bands derived from multitemporal Sentinel-2A imagery (10 bands for each of the three sub-periods within the year). The model was trained on 89,986 labeled LULC points linked to explanatory variables, and its training performance was assessed using 100-fold cross-validation. After training, the classifier was applied to predict LULC classes within a 250 m buffer zone along ephemeral rivers draining catchments of at least 1000 km^2, using the full set of 30 spectral bands.

The initial classification results revealed misclassification errors between the "*Water*" and "*Vegetation*" classes. The analysis of the Maxar ground truth imagery revealed that stagnant water bodies in ephemeral riverbeds often appear greenish due to algal bloom (see Fig. 4d; Akin-Oriola et al., 2006), which leads to spectral confusion with vegetated surfaces (Codjia et al., 2025). To address this, the "Water" class was redefined based exclusively on dry-season conditions using the Modified Normalized Difference Water Index (MNDWI), calculated from Sentinel-2 imagery. A calibrated MNDWI threshold ≥ -0.1, specifically adapted to the West African Sahel context was applied (Girard et al., 2025). While MNDWI typically yields positive values for open water and negative or near-zero values for vegetation and soil thereby enhancing water body classification, the lower threshold used here accounts for regional conditions such as shallow or turbid water bodies that may not reach positive MNDWI values. The MNDWI (Xu, 2006) was calculated as in Equation (5):

$$MNDWI = \frac{Green - SWIR1}{Green + SWIR1} \tag{5}$$

where Green and SWIR1 represent the surface reflectance values in the green and shortwave infrared (SWIR1) bands, respectively.

The Random Forest classifier was finally trained on 57,157 LULC class points (excluding the water class) to classify land cover types within the buffer zones. To produce the final LULC classification, the water class was first independently extracted using the calibrated MNDWI threshold. This binary water mask was then overlaid onto the Random Forest classification of the remaining classes (sandy riverbeds, bare soil, and vegetation), using a hierarchical rule whereby all pixels identified as water by MNDWI were systematically assigned to the 'Water' class, regardless of their Random Forest prediction. Consequently, in cases where a pixel was predicted as 'non-water' by the Random Forest but exceeded the MNDWI water threshold, the MNDWI-based classification took priority. This ensured a consistent and physically meaningful separation between open water surfaces and other land cover types. The predictive performance

of the final classification was assessed against the 1766 predefined validation points (Fig. 4) through the construction of a confusion matrix, using metrics presented in **SM** Table S4. To complement these accuracy metrics, we also estimated the uncertainty associated with each per-class sensitivity and precision values. Confidence intervals were computed from the observed proportions of correctly and incorrectly classified points for each land cover class, using standard 95 % binomial confidence interval estimation based on Wilson (1927), which provides a robust measure of the variability expected due to sampling.

While the LULC classification developed in this study effectively delineates surface LULC, it does not directly capture the presence of shallow groundwater within the beds of ESRs. To address this limitation, the third objective of the study focused on characterizing the potential water storage capacity of ESRs (**Step 6 –** Fig. 2). This was accomplished by integrating vegetation information derived from the LULC classification with riparian canopy height data from Tolan et al. (2024), originally at a 1 m resolution and resampled (mean of neighboring pixels) to 10 m to ensure compatibility with the other spatial layers.

Dense riparian vegetation persisting along riverbeds during the dry season is widely recognized as a proxy for shallow groundwater availability, providing indirect evidence of subsurface water presence (Castellazzi et al., 2024; Cunningham et al., 2011; Schilling et al., 2021; Wang et al., 2023). Accordingly, ESR segments were selected by overlaying the ephemeral river network (drainage area $>1000\ km^2$) with the classified LULC map. Thus, portions of the ephemeral river network that do not overlap with pixels belonging to the "*Sandy riverbed*" class in the LULC map were not selected. From the selected ESR segments (total length: 2120 km), a more detailed identification of potential shallow groundwater zones was conducted by isolating vegetation pixels within the 250 m buffer zone. Only

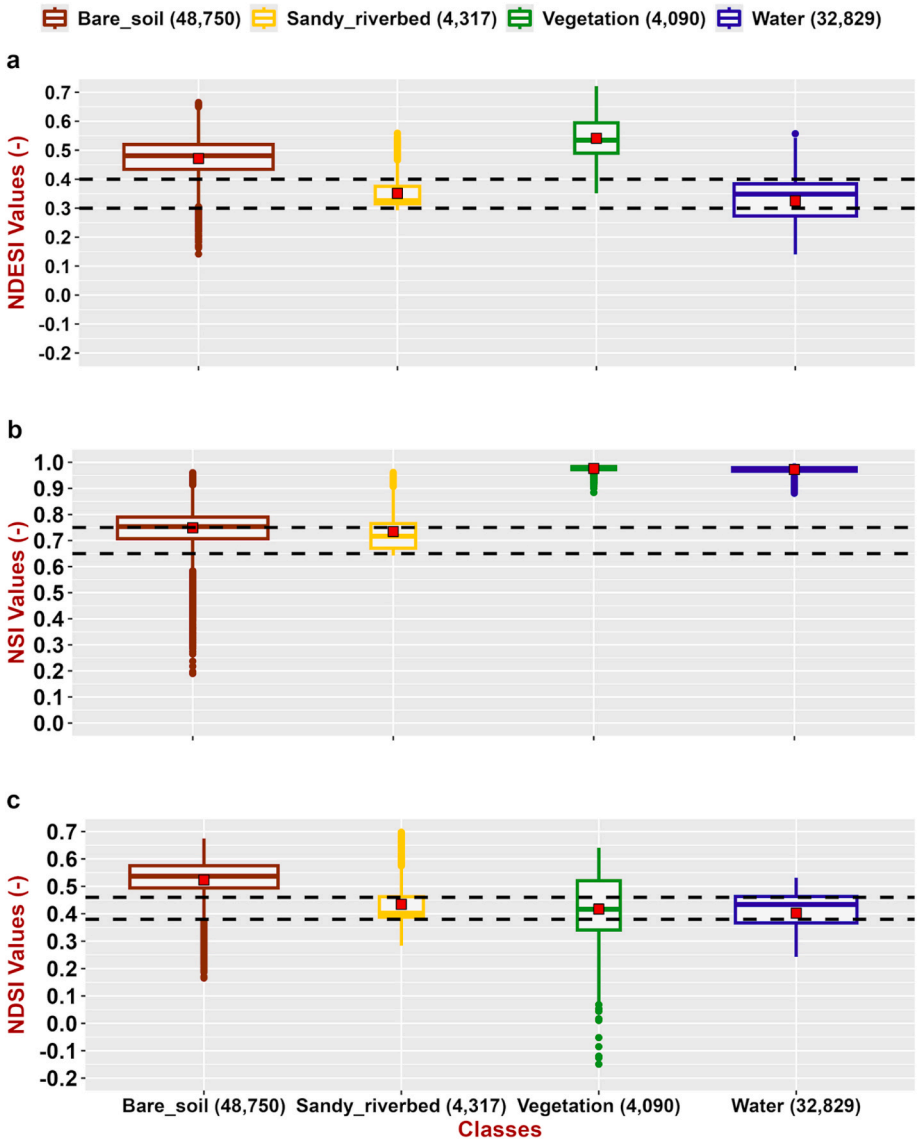

Fig. 5. Distribution of spectral indices characteristic of sand according to different LULC (89,986 training sampled points). The width of the boxplots is proportional to the number of samples.

pixels classified as vegetation in the supervised classification (LULC map), surrounded by a minimum of 8 neighboring vegetation pixels (to exclude isolated vegetation patches), and exhibiting a canopy height equal to or greater than 5 m were retained. The 5 m threshold was adopted to exclude seasonal herbaceous vegetation and to specifically capture taller perennial woody species, which are reliable indicators of shallow groundwater access in riparian corridors (see Table 2, Shakhane et al., 2017). These pixels therefore indicate the presence of perennial riparian vegetation likely sustained by shallow groundwater. Finally, ESR segments (total length: 402 km) were classified as having potential for shallow groundwater occurrence when their 250 m buffer contained at least 30 such pixels indicative of perennial riparian vegetation.

In addition, to incorporate the human dimension of groundwater accessibility, the 100 m resolution WorldPop (2020) population dataset was overlaid with the previously identified ESR segments. We used constrained top-down WorldPop population estimates to prevent the incorrect assignment of population to uninhabited land areas (Messager et al., 2021). Focal statistics were applied to calculate the total population count within a 5 km radius around each ESR centerline segment. Previous water-access studies in Sub-Saharan Africa commonly use buffer distances of up to 1 km to represent immediate access to drinking water (Nygren et al., 2016). However, such narrow buffers may fail to capture populations potentially reliant on nearby water sources in more sparsely populated or rural areas. Moreover, in the context of irrigation, which could potentially be developed along ESRs, a 5 km buffer appears appropriate. Ultimately, we adopt a 5 km buffer as a balanced compromise, considered broad enough to encompass relevant population clusters associated with each ESR segment. Combined with riparian vegetation and canopy height data this allows an assessment of areas where shallow groundwater resources may be accessible to nearby communities.

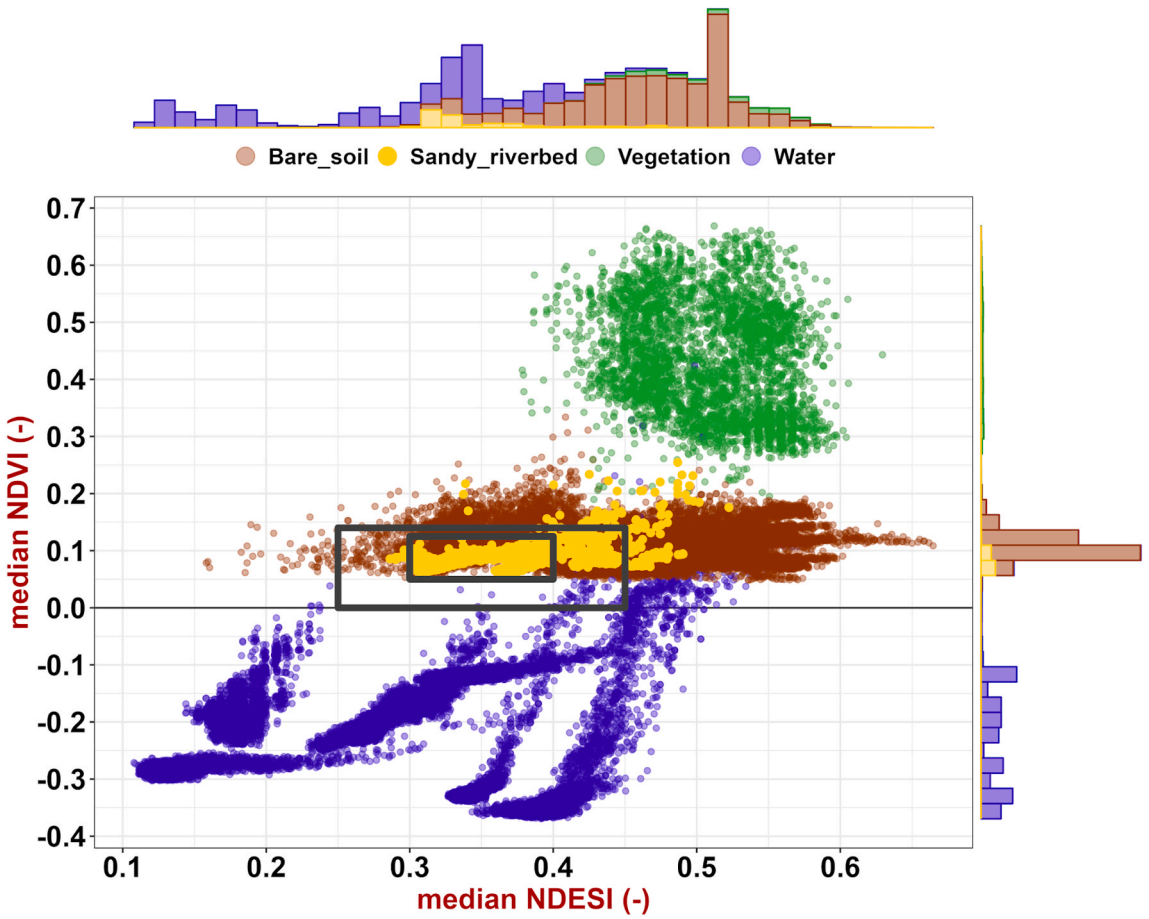

Fig. 6. Biplot of median NDVI versus median NDESI values for the different sample points. The marginal histograms (top and right) show the distribution of each class. The majority of Sandy riverbed samples cluster within the interval 0.3–0.4 for median NDESI and 0.05–0.125 for median NDVI, corresponding to the restrictive composite threshold (CT1, small black rectangle). The extended composite threshold (CT2) is indicated by the larger black rectangle.

3. Results

3.1. Spectral indices characterizing ephemeral sand rivers

The calculation of spectral indices yields single-band grayscale images, where pixel intensity reflects the index values; see **SM** Fig. S9–S11 for descriptions. The distribution of sand-specific spectral indices (Table 2) across various LULC categories (89,986 training sampled points) is illustrated in Fig. 5.

The analysis of Fig. 5 allowed for the visual definition of intervals for each spectral index that maximize the capture of the "*Sandy_riverbed*" class while minimizing the presence of the "*Bare_soil*" class. The other classes (Water, Vegetation) are subsequently discriminated using a spectral index–NDVI biplot (Fig. 6). For the NDESI, approximately 86 % of the training samples identified as sandy riverbeds fall within the 0.3–0.4 interval. However, this range also captures a considerable proportion of the *Water class* (51 %), along with smaller overlaps from *Bare soil* (14 %) and *Vegetation* (0.42 %) (Fig. 5a). In the case of the NSI, about 67 % of sandy riverbed samples are concentrated between 0.65 and 0.75. This interval also overlaps with substantial fractions of the *Bare soil* (37 %) classes, while the *Vegetation* and *Water class* are absent (0 %) (Fig. 5b). For the NDSI, 75 % of sandy riverbed samples are confined to the 0.38–0.46 range, which also coincides with 32 % of both *Water* and *Vegetation* samples, and 14 % of *Bare soil* samples (Fig. 5c).

Among the three indices, NDESI demonstrates the strongest discriminative capacity, as it captures the largest proportion of sandy riverbed samples within its threshold range. Moreover, when combined with NDVI in a biplot representation, a clearer separation emerges between the *Water* and *Vegetation* classes, improving class discrimination (Fig. 6).

Based on this distribution (Fig. 6), two sets of composite thresholds were defined visually:

- A restrictive threshold (CT1): $0.3 \leq$ median NDESI ≤ 0.4 and $0.05 \leq$ median NDVI ≤ 0.125.
- An extended threshold (CT2): $0.25 \leq$ median NDESI ≤ 0.45 and $0 \leq$ median NDVI ≤ 0.14.

CT1 is limited to capturing the area where the "*Sandy riverbed*" class is concentrated while minimizing the inclusion of the "*Bare_Soil*" class, whereas CT2 considers wider NDESI and NDVI intervals to capture more "*Sandy_riverbed*" points at the expense of including a substantial number of points from other classes. Applying CT1 to the training samples correctly identified 86 % of sandy riverbed points (true positives), with 14 % remaining undetected (false negatives). Misclassification was substantially reduced, with false positives limited to 7.3 % for Bare soil and 0 % for both Vegetation and Water (Table 4, Fig. 6). In contrast, applying CT2 improved the detection rate, correctly identifying 93 % of sandy riverbed points, while reducing false negatives to 7 %. However, this broader interval increased misclassification, with false positives reaching 32 % for *Bare soil*, 0 % for *Vegetation*, and 0.2 % for *Water* (Table 4, Fig. 6).

CT1 and CT2 were subsequently applied over the buffer zones delineated across the study area. Out of the 1766 validation points established throughout the study area, 351 correspond to sandy riverbeds (Fig. 4). When applied at a broader scale across the defined buffer zones, CT1 detected only 149 of the sandy riverbed validation points, corresponding to a sensitivity of approximately 42 % and a precision of 92 % (**SM** Fig. S12a), an insufficient detection rate for accurate mapping. In contrast, CT2 detected 251 of these points, corresponding to a sensitivity of approximately 72 % and a precision of 72 % (**SM** Fig. S12b), a satisfactory detection rate for accurate mapping, though with an increased risk of false positives.

Fig. 7a illustrates the limited performance of the spectral index classification using CT1. Only a few segments of sandy riverbeds are correctly detected (true positives), while a large portion of the riverbed remains undetected (false negatives). Additionally, small areas outside the actual river channels are misclassified as sandy riverbed surfaces (false positives). In contrast, Fig. 7b shows the results with CT2, which captures a substantially larger portion of the sandy riverbeds, leaving only a few sections undetected (false negatives). However, this improvement comes at the cost of increased misclassification, with larger areas outside the river channels being identified as sandy riverbed surfaces (false positives).

The results show that identifying sandy rivers exclusively from spectral indices is not sufficiently accurate, indicating that additional methods need to be explored.

3.2. LULC supervised classification

The ephemeral rivers (with a catchment area larger than 1000 km^2) identified across the study area using the random forest classifier have a combined total length of 31,287 km (**SM** Fig. S5). The supervised classification exhibits excellent training performance, achieving an accuracy of 0.99, demonstrating that the model adapts well to the various configurations of the dataset. Within

Table 4
Distribution of training sample points across Land Use/Land Cover (LULC) classes within the composite thresholds CT1 and CT2.

LULC Classes	Number of identified points CT1 | CT2	Total training points	Proportion (%) of data CT1 | CT2
Sandy riverbed	3,713 | 4,032	4,317	86.0 | 93.0
Bare soil	3,566 | 15,798	48,750	7.3 | 32.0
Vegetation	0 | 0	4,090	0.0 | 0.0
Water	1 | 77	32,829	0.0 | 0.2
Total	7,280 | 19,907	89,986	8.0 | 22.0

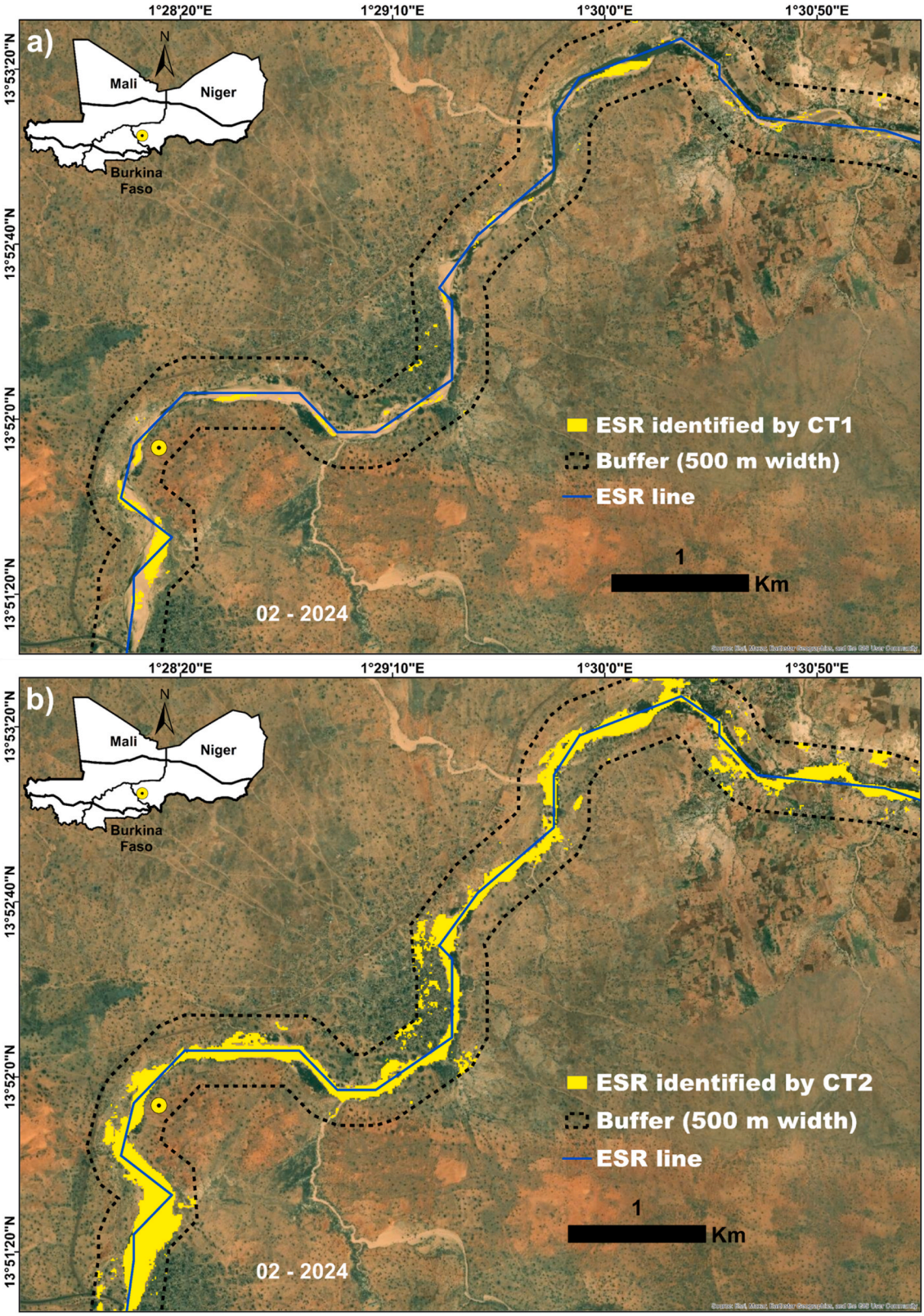

Fig. 7. High-resolution image of a site identified in Niger, showing an ephemeral sand river and the surrounding land cover (0.5 m resolution, February 2024). The ephemeral sand river is delineated using CT1 (a) and CT2 (b).

the defined buffer zones, the supervised classification results indicate that, out of 36,260,458 pixels, sandy riverbeds account for 14.57 %, bare soil for 37.60 %, vegetation for 37.54 %, and water for 10.29 %.

Based on the independent validation points (Fig. 4), the classification achieved an overall accuracy of 0.92, indicating a robust model performance. High F1-scores were obtained across all classes (Table 5): Sandy riverbed (0.90), Bare soil (0.86), Vegetation (0.96), and Water (0.93).

Regarding the "*Sandy riverbed*" class, the sensitivity (0.89) indicates that 89 % of true sandy riverbed points were correctly identified, while the precision (0.91) shows that 91 % of the points classified as "*Sandy riverbed*" indeed belong to this category. Some confusion with the "*Bare soil*" class was observed, with 35 points misclassified. This level of misclassification is acceptable, given the inherent difficulty in distinguishing between sandy riverbed surfaces and bare soils: the spectral similarity between these two classes, particularly where golden sands are present within the "Bare soil" category, likely contributed to this confusion.

For the "*Vegetation*" class, classification performance is excellent, with a sensitivity of 0.94 and a precision of 0.99. Only 24 vegetation points were misclassified as "*Bare soil*" likely due to sparse vegetation cover leading to reduced chlorophyll absorption signals. For the "*Bare soil*" class, sensitivity was very high (0.97), indicating that nearly all bare soil points were correctly detected. However, the precision was comparatively lower (0.78), suggesting that a significant number of points predicted as "*Bare soil*" were actually from other classes, particularly "*Water*" (49 misclassified points).

Concerning the "*Water*" class, the classification achieved a high sensitivity (0.88) and an excellent precision (0.99), indicating that almost all points classified as "*Water*" truly belong to this category. Nonetheless, some confusion was observed, with 49 "*Water*" points misclassified as "*Bare soil*" and 15 as "*Sandy riverbed*". It should be noted that the "*Water*" class was extracted using the MNDWI spectral index and merged with the RF model prediction (Sandy riverbed, Sandy soil, Vegetation) to produce the final classification. This misclassification likely arises from spectral variability due to soil moisture, especially in areas spatially close to water bodies. Overall, the confusion matrix demonstrates strong model performance, with high precision ($\geq$0.78) and generally very good sensitivity ($\geq$0.88). Minor misclassifications primarily occurred between "*Bare soil*" and "*Sandy riverbed*" and between "*Bare soil*" and "*Water*".

The spectral profiles of the three LULC classes (i.e. sandy riverbed, bare soil, and vegetation) exhibited significant temporal variation across the three seasonal sub-periods considered: dry (February–May), humid (June–September) and transition (October–January) periods (Fig. 8). During the dry period (Fig. 8a), spectral profiles are characterized by high reflectance values in the visible and near-infrared (NIR) regions for both sandy riverbeds and bare soils. *Sandy riverbeds* show the highest reflectance, particularly in the shortwave infrared (SWIR) bands. *Bare soil* exhibits a similar behavior but with slightly lower reflectance values across all bands. *Vegetation* displays low reflectance in the visible region, driven by chlorophyll absorption, followed by a sharp rise in the NIR, typical of healthy vegetation, while remaining relatively low in the SWIR due to limited water content.

During the humid period (Fig. 8b), significant changes occur. *Sandy riverbeds* and *bare soils* exhibit a general reduction in reflectance across all spectral bands, most notably in the SWIR, reflecting increased moisture content and potential sediment deposition. *Vegetation* shows a substantial increase in NIR reflectance, indicating higher biomass and chlorophyll activity, while SWIR absorption features become more pronounced, reflecting elevated leaf water content.

In the transition period (Fig. 8c), spectral responses are intermediate between the dry and humid conditions. *Sandy riverbeds* and *bare soils* display reflectance values slightly lower than in the dry period but higher than during the humid period, suggesting gradual moisture loss. *Vegetation* NIR reflectance remains elevated compared to the dry season but does not reach the peak values observed during the humid period, indicating a decline in photosynthetic activity as rainfall diminishes.

It is important to note that the "*Water*" class was derived separately using the MNDWI index and was not directly included in the supervised classification model; thus, its spectral signature was not part of the training process.

A visual comparison between Figs. 8 and 9 shows that the classification results in Fig. 9 for the selected site in Niger accurately capture both the presence and spatial extent of the ESR and the other land-cover classes. For the vegetation class, the model successfully identifies areas of dense vegetation; however, isolated or scattered trees are typically classified as bare soil. Consequently, areas that do not correspond to either ESRs or dense vegetation are also predicted as bare soil. These classification results reflect typical dry-season surface conditions.

Table 5
Confusion matrix resulting from the validation of the classification result on the 1766 validation points distributed across the study area (Fig. 4).

Confusion matrix (O)		Predicted LULC classes						
		Sandy riverbed	Bare soil	Vegetation	Water	Total	Sensitivity	CI_{95}
Observed LULC classes	**Sandy riverbed**	**311**	**35**	**3**	**2**	**351**	**0.89**	**[0.85, 0.92]**
	Bare soil	**9**	**377**	**2**	**0**	**388**	**0.97**	**[0.95, 0.98]**
	Vegetation	**5**	**24**	**477**	**0**	**506**	**0.94**	**[0.92, 0.96]**
	Water	**15**	**49**	**1**	**456**	**521**	**0.88**	**[0,84, 0.90]**
	Total	**340**	**485**	**483**	**458**	**1766**		
	Precision	**0.91**	**0.78**	**0.99**	**0.99**			
	CI_{95}	**[0.88, 0.94]**	**[0.74, 0.81]**	**[0.97, 0.99]**	**[0.98, 1.00]**			

Note. The number of correctly predicted points is read along the diagonal. The CI95 column refers to the 95 % confidence intervals computed using Wilson binomial proportion intervals based on the confusion-matrix sample size for each class (Wilson, 1927).

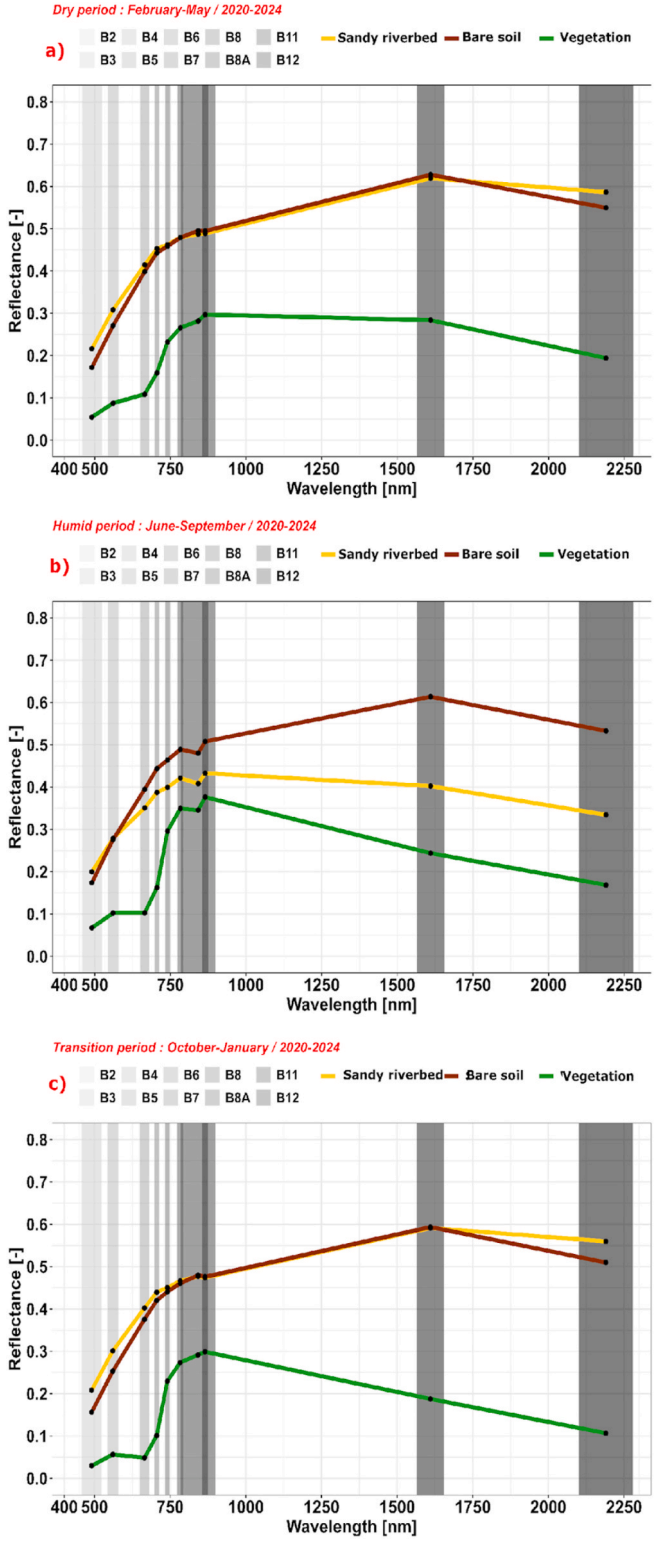

Fig. 8. Spectral signature of different classes (sandy riverbed, bare soil, vegetation) according to various periods: dry (a), wet (b), and transitional (c) from 2020 to 2024.

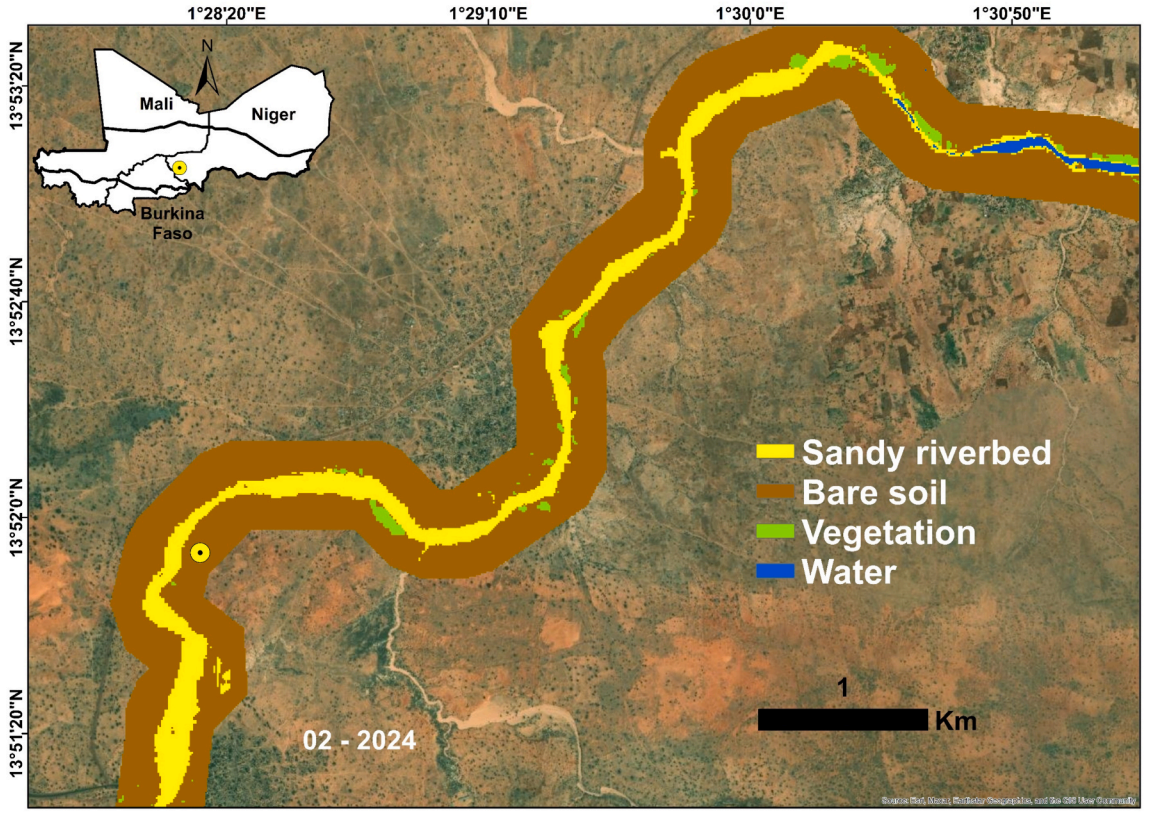

Fig. 9. LULC classification results of the identified site in Niger. Background: ArcGIS Pro, Maxar Imagery (0.5m resolution, February 2024).

3.3. Population and riparian vegetation along ephemeral sand rivers

By overlaying the results of the supervised LULC classification with the mapped ephemeral river network, it was possible to isolate and select river segments corresponding specifically to ESRs. The total length of rivers draining at least 1000 km^2 within the study area of interest (Fig. 1) is estimated at 40,101 km, of which 78 % are ephemeral rivers. Thus, ephemeral rivers (draining at least 1000 km^2 catchment area) have a total length of 31,287 km (**SM** Fig. S5), of which 7 %, i.e., 2120 km, correspond to segments (with a minimum length of 20 m) identified as ESRs (Fig. 10). Applying a 5 km buffer wide around these ESR segments over gridded population datasets allowed for an estimation of the riparian population, totaling 7.4 million individuals across the study area, representing 12 % of the total population of the three countries combined, with 1.1 million in Burkina Faso, 1.5 million in Mali, and 4.8 million in Niger. The notably higher population in Niger is primarily attributable to the proximity of certain ESRs to the national capital, whereas in Burkina Faso and Mali, these rivers are generally located farther from major urban centers.

While supervised classification enabled the spatial delineation of ephemeral sand rivers (ESRs), it did not on its own provide direct evidence of shallow groundwater occurrence within their channels. To address this limitation, riparian vegetation patterns (i.e., Vegetation class) derived from the supervised classification were combined with canopy height data as proxies for groundwater accessibility (see Section 2.4). The analysis revealed that dense, perennial riparian vegetation with canopy heights above 5 m occurred along 402 km of ESR segments, representing 19 % of the total mapped ESR length. These segments were therefore interpreted as zones with a high likelihood of shallow groundwater storage (see Section 2.4), as the persistence of tall woody vegetation during the dry season is a well-established indicator of sustained subsurface water availability in arid and semi-arid environments (Wang et al., 2023).

Fig. 10 presents the geographic distribution of the identified ephemeral sand rivers (ESRs) with high potential for shallow groundwater presence, accompanied by high-resolution satellite imagery illustrating the spatial relationship between riparian vegetation and adjacent ESRs. In Fig. 10, the alternating display of green lines (ESRs with high potential for shallow groundwater presence) and blue lines (ephemeral rivers with catchment areas >1000 km^2) results from slight misalignments between the river network and the actual river course observed in high-resolution imagery. As a result, some vegetated river segments that likely correspond to true ESRs were not spatially intersected with the classified sandy riverbed pixels and were therefore not selected as ESRs with groundwater potential. This implies that the reported 402 km of high-potential ESRs should be regarded as a conservative estimate. While a precise quantification of the missed ESR length is not currently possible without a systematically corrected river network and field validation, visual inspection of high-resolution imagery suggests that these omissions remain localized and do not affect the large-scale spatial patterns identified. Consequently, the associated riparian population estimates near high-potential ESRs should also be interpreted as

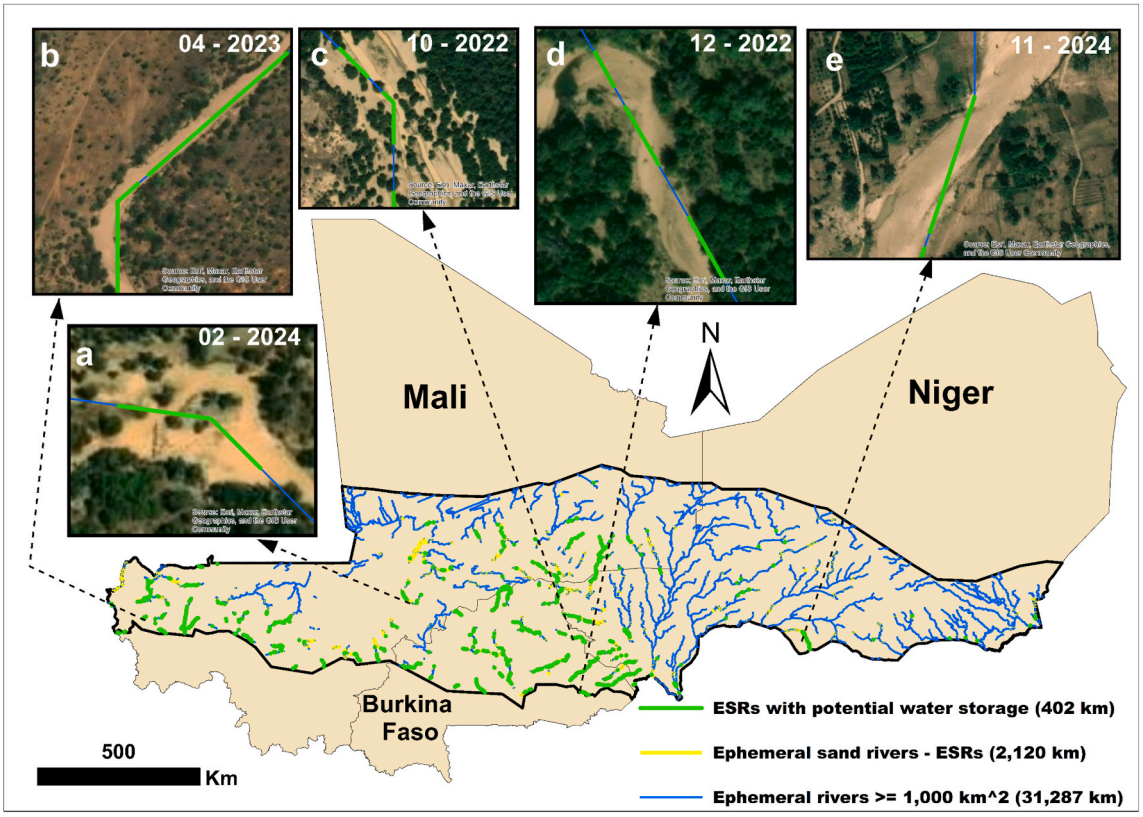

Fig. 10. Representation of identified ephemeral sand rivers (ESRs) with high potential for shallow groundwater presence (green lines). For visualization purposes, ESRs with potential water storage are displayed with a thicker line width compared to the remaining ESRs, which may give the impression that they account for more than half of the total ESR network length.

lower-bound approximations. For detailed satellite-based visualizations of the identified high-potential ESR segments with shallow groundwater occurrence, see the **Data availability section**.

Within a 5 km radius of these sites, predominantly located in rural areas, the total riparian population close to sand rivers with water storage potential is estimated at 3M individuals or nearly 41 % of those living close to all sand rivers identified, with 0.7M in Burkina Faso, 0.6M in Mali, and 1.7M in Niger.

4. Discussion

4.1. Key findings

This study assessed the potential of several spectral indices (NDESI, NSI, NDSI) for large-scale detection of ESRs. Although these indices allowed visual identification of sandy riverbeds in some areas (**SM** Fig. S9–S11, Fig. 7), consistent detection was hindered by spectral confusion between "*Sandy riverbed*" and "*Bare soil*" classes. Among them, the NDVI–NDESI combination performed best, with detection accuracy ranging from 42 % to 72 %. Similarly, by Bremer (2022) highlighted the relevance of NDESI for ESR detection in Zimbabwe, Kenya, and Ethiopia, though with higher thresholds (NDESI <0.6 and NDVI <0.3) than those found here. These differences likely reflect environmental variability among sites (Marzouki and Dridri, 2022), including contrasts in climate, vegetation, and sand spectral properties between the Sahel and southern Africa.

Compared to the direct use of spectral indices for sandy riverbed detection, supervised classification provided higher mapping accuracy, achieving an overall accuracy of 0.92 and F1-scores exceeding 0.86 across all LULC classes, albeit at the expense of greater computational and processing time requirements. In situations where rapid ESR assessments are required in Sahelian regions and prior riverbed information is unavailable, spectral indices, particularly the threshold developed in this study (CT2), may serve as a valuable first-order tool for coarse and rapid mapping, whereas supervised classification can deliver more accurate and detailed results (Belgiu and Drăguţ, 2016; Yonaba et al., 2021).

The results demonstrate that relying on a single Sentinel-2 image for supervised classification, whether from the dry, humid, or transition period, limits the accurate discrimination of surface classes due to seasonal spectral similarities, whereas incorporating multi-temporal imagery from these periods markedly enhances spectral discrimination (see **SM** Table S5). For instance, during the dry period, sandy riverbeds and bare soils exhibit very similar spectral signatures, increasing the risk of misclassification. In contrast,

during the humid period, the enhanced contrast in the SWIR bands facilitates the separation between bare soil and sandy riverbeds, while the dry and transition periods are more suitable for distinguishing vegetation. Fig. 8b suggests that the humid period, rather than the dry period, may provide better accuracy for spectral index (NDESI, NDSI, NSI) analyses used to discriminate sandy riverbeds.

In this study, 402 km i.e., 19 % of ESRs length were identified as having high potential for groundwater accessibility. Within a 5 km radius of these sites, approximately 3 million individuals, predominantly in rural areas, live near potential groundwater resources. These results underscore the strategic role ESRs can play in enhancing rural resilience to climate variability, in supporting off-season agriculture and sustaining livelihoods during dry periods (Castelli et al., 2018; Eisma and Merwade, 2021). Furthermore, infrastructure interventions such as sand dams and subsurface gabion weirs can enhance water storage capacity by promoting aquifer recharge while offering a cost-effective and environmentally sustainable alternative to large-scale dam construction (Lazurko et al., 2024; Love et al., 2011). While these figures provide valuable regional-scale insight, they should be interpreted as best estimates rather than precise measurements. The total ESR length results from the aggregation of spatially scattered segments derived from classified imagery, for which statistical uncertainty cannot be robustly propagated. Likewise, the population count reflects the characteristics of the WorldPop dataset and is intended as an indicative exposure estimate rather than a value with quantifiable confidence bounds.

Beyond its direct implications for water and agricultural development, this study demonstrates how the integrated use of DEM-based hydrological analysis, sand-sensitive spectral indices, and multi-temporal LULC classification (using Random Forest technique) can substantially advance the large-scale mapping of ESRs in data-scarce dryland regions. In environments where in-situ hydrological measurements, sediment surveys and groundwater monitoring are extremely limited, the proposed framework provides a scalable, transferable and operational solution for identifying subsurface water storage zones using only openly accessible Earth observation and topographic datasets. The explicit coupling of hydrological connectivity (from DEM analysis), surface sediment characterization (from spectral indices) and robust machine-learning-based land cover mapping, the approach overcomes the limitations of single-data-source methods that are often unreliable in Sahelian environments (Yonaba et al., 2021).

The resulting ESR inventory constitutes not only an advocacy tool for national governments, development partners and NGOs, but also a spatially explicit decision-support instrument for guiding water resource planning and investment in arid and semi-arid regions. By identifying specific river segments where shallow groundwater storage is most likely, the approach enables the prioritization of locations for supplementary irrigation, livestock watering and domestic water supply within national and sub-national water development strategies. This information can directly support the design of climate adaptation programs, rural irrigation schemes and drought resilience investments by reducing exploration uncertainty and targeting interventions where hydrological returns are most likely. Practical investments such as hand-drilled well points, subsurface infiltration structures and small-scale abstraction systems coupled with local capacity building, can thus be implemented in a more spatially targeted, risk-informed and cost-effective manner, contributing to improved food security and rural resilience across the West African Sahel (Prasad et al., 2023, 2024).

A further major strength of this study lies in its full reliance on open-access data and tools. All input datasets, the derived ESR inventory, and the associated visualization products are made openly available through a dedicated Zenodo repository (https://doi.org/10.5281/zenodo.17398126) and an interactive Google Earth Engine (GEE) web viewer (https://axelbelemtougri.users.earthengine.app/view/a4store-sand-rivers-project), ensuring full transparency, reproducibility, and immediate usability by both the scientific community and operational stakeholders. This open-science approach significantly enhances the transferability of the proposed methodology to other data-scarce dryland regions worldwide.

4.2. Limitation of the study and potential applications

Several limitations must be acknowledged in this study, which may influence the accuracy and broader applicability of the proposed methodology.

First, the workflow used in this study was designed to ensure internally consistent and hydrologically plausible results. However, the sensitivity of several methodological choices could be examined more systematically in future work. The exploratory testing of various DEM sources (MERIT, AW3D) and contributing area thresholds for river network extraction were considered in this study to ensure the alignment with reference hydrographic datasets. We also acknowledge that the temporal aggregation through the use of multiyear median composites may influence the spectral contrasts that define ESR detectability. A comprehensive quantitative sensitivity analysis of these components, including DEM selection, drainage-area thresholds and temporal compositing strategies would therefore offer valuable insights into the robustness and transferability of the ESR mapping framework. Such analyses, however, fall beyond the scope of the present work, whose primary objective was to produce the first regional-scale inventory of ESR across the Sahel.

In some areas, river segments were classified as sandy riverbeds where green algal mats covered the surface, as observed in high-resolution Maxar imagery, which limits the direct optical confirmation of the underlying sedimentary substrate. In such cases, the true nature of the riverbed material (sand versus fine-grained alluvium) cannot be reliably confirmed from optical remote sensing alone. Targeted field validation therefore constitutes a critical next step to verify both the physical presence of sandy substrate and the predictive accuracy of the proposed ESR detection framework. Field investigations combining visual inspection, shallow augering, sediment sampling, and basic hydro-geophysical measurements (e.g., electrical resistivity profiling) would allow confirmation of sand thickness, grain size, and shallow groundwater occurrence, as recommended in similar ESR studies (Cunningham et al., 2011; Mpala et al., 2016). Such validation would further strengthen confidence in the derived ESR inventory and in the prioritization of sites for future water development interventions.

Second, the use of multispectral Sentinel-2A imagery, despite its advantages of free access and relatively high spatial resolution (10 m), limits spectral discrimination between certain land cover classes. The integration of hyperspectral data, capturing finer spectral

details, could significantly improve the differentiation between vegetation, bare soil, sand, and algal-covered surfaces (Li et al., 2024; Marzouki and Dridri, 2022). Future research could leverage emerging hyperspectral sensors, or the combination of SAR (Synthetic Aperture Radar) and optical imagery, to enhance classification performance.

Although the Random Forest (RF) algorithm demonstrated strong performance in this study, alternative machine learning methods, particularly deep learning approaches such as Convolutional Neural Networks (CNNs), could potentially yield superior results. CNNs are capable of learning complex spatial hierarchies and contextual information and have been successfully applied in similar LULC classification contexts (Belgiu and Drăguţ, 2016; Thirumalraj et al., 2023).

The study relied on official hydrographic networks from Burkina Faso and Mali, as well as an enhanced river network dataset derived from remote sensing for Niger, to delineate river networks. However, spatial misalignments between digitized river traces and actual riverbeds observable in satellite imagery were noted in many areas. These discrepancies may have led to the omission of sandy rivers not spatially aligned with the reference datasets. Improved river network datasets, derived from recent high-resolution DEMs and up-to-date optical imagery, would enhance future riverbed mapping efforts. In addition, the spatial resolution of the DEM (90 m) and the selected upstream contributing area threshold (2.5 km^2) may introduce uncertainties in the delineation of ephemeral river segments. These choices may locally lead to either an overestimation of ESR extent through the inclusion of minor drainage features, or an underestimation through the omission of narrower or weakly expressed channels, particularly in low-relief or sediment-dominated landscapes.

Inferences of shallow groundwater presence based on canopy height data were occasionally limited by missing or inaccurate measurements, leading to the exclusion of some vegetated sandy river sites from the final groundwater potential inventory. In particular, areas lacking 5 m canopy height data within the 250 m buffer could not be confirmed as groundwater-sustained vegetation zones. Enhancements to canopy height datasets would thus improve groundwater proxy identification.

Furthermore, while web-based visualization platforms facilitate the dissemination and exploration of ESR potentials, the high-resolution imagery (e.g., Maxar or WorldView-2) used for model validation is not openly accessible. Freely available imagery such as Google Maps often lacks the spatial and temporal resolution necessary for fine-scale validation of ground features.

Despite these limitations, the methodology presented here offers considerable promise as 19 % of ESRs length have been identified as potential groundwater storage areas, offering significant value for climate-resilient agriculture and water management initiatives in the Sahel. Prior to operational implementation, ground-based hydro-geophysical investigations such as electrical resistivity surveys and test drilling by hand are recommended to verify subsurface water availability at the selected sites. Given the security challenges prevalent across parts of the Sahel, any field-based interventions should be preceded by cross-referencing spatial information from this study with national security risk assessments.

5. Conclusion

This study presents a remote sensing, GIS, and machine learning-based methodology for the detection and mapping of ESRs in the West African Sahel. By using supervised classification, and hydrological analysis, the approach successfully identifies ESRs with high potential for shallow groundwater storage. The methodology combines open-access datasets with robust geospatial and statistical techniques, offering a scalable and cost-effective framework for water resource assessment in arid and semi-arid environments.

The high accuracy achieved through supervised classification (overall accuracy of 0.92) underlines the robustness and relevance of the proposed method for the accurate identification of sandy riverbeds. Furthermore, the integration of riparian vegetation and canopy height as proxies for shallow groundwater availability provides a valuable, non-invasive approach for prioritizing intervention zones, ultimately leading to the identification of 402 km length of ESRs with potential water storage.

These findings highlight the significant but still underutilized potential of ephemeral sand rivers to support dry-season agriculture and enhance rural water security in the Sahel, a region increasingly affected by climate variability and demographic pressures. With an estimated 3 million people living within 5 km of ESRs identified as having high potential for shallow groundwater access, targeted investments in water-harvesting structures and small-scale irrigation could substantially strengthen rural livelihoods, food security, and climate resilience. These results should, however, be interpreted with caution. The mapped ESR extent and associated population estimates rely on multi-source geospatial datasets whose uncertainties cannot be fully quantified, and some methodological choices (including such as DEM selection or temporal aggregation) of satellite images for LULC mapping) were not subjected to formal sensitivity analysis.

Future research should focus on refining this methodology through systematic field validation, the incorporation of hyperspectral and SAR data, and the adoption of advanced AI-driven models such as convolutional neural networks. Additionally, integrating this approach into broader water resource planning and rural development frameworks will be essential to promote the sustainable and equitable use of these hidden groundwater reserves across the Sahel. Although these reserves are replenished each rainy season, it is crucial to ensure a sustainable yield, as excessive extraction could negatively impact riparian vegetation.

CRediT authorship contribution statement

Axel Belemtougri: Writing – original draft, Methodology, Formal analysis, Data curation, Conceptualization. **Roland Yonaba:** Writing – original draft, Methodology, Formal analysis, Conceptualization. **Claire I. Michailovsky:** Writing – review & editing, Supervision, Methodology, Conceptualization. **Tibor Stigter:** Writing – review & editing, Supervision, Methodology, Conceptualization. **Lawani Adjadi Mounirou:** Writing – review & editing, Methodology, Formal analysis. **Pieter van der Zaag:** Writing – review & editing, Supervision, Methodology, Funding acquisition, Conceptualization.

Ethical statement

The authors confirm that this manuscript represents original research that has not been published previously and is not under consideration for publication elsewhere. All authors made substantial contributions to the research and manuscript preparation, and have reviewed and approved the final submitted version. The study did not involve human participants, animals, or any experimental procedures requiring ethical approval. The work fully adheres to Elsevier's publication ethics and integrity guidelines, and all analyses were conducted in accordance with the principles of academic integrity.

Declaration of generative AI

During the preparation of this work the authors used OpenAI's ChatGPT 5 in order to assist with drafting, language refinement, and improving the clarity and flow of the manuscript. After using this tool, the authors critically reviewed and edited the content as needed and take full responsibility for the content of the published article.

Funding and acknowledgments

The authors gratefully acknowledge IHE Delft for supporting this research, which was carried out within the framework of the A4Store project (Smallholder farming families Adapt African Alluvial Aquifers to Strengthen Their Own Resilience). The A4Store project aims to tackle the challenges African countries face due to climate change and rapid population growth. It explores the potential of enhancing the prosperity and resilience of vulnerable, resource-poor rural households in fragile African drylands through nature-based water storage in ESRs for sustainable food production. More at https://sandrivers.org/a4store/.

Declaration of competing interest

The authors declare that they have no known competing financial interests or personal relationships that could have appeared to influence the work reported in this paper.

Appendix A. Supplementary data

Supplementary data to this article can be found online at https://doi.org/10.1016/j.rsase.2025.101838.

Data availability

The final model prediction results, environmental covariates related to vegetation and population, as well as the geographic characteristics of the study area, are displayed on the Google Earth Engine platform at the following link: https://axelbelemtougri.users.earthengine.app/view/a4store-sand-rivers-project.

This interactive web-based tool allows users to explore various layers that support the assessment of the area's potential suitability for promoting smallholder irrigation using water stored in the alluvial aquifer. A GitHub link providing full access to all scripts used for the derivation of spectral indices and the implementation of the Random Forest models in Google Earth Engine is available at the following link: https://github.com/falltok/Mapping_Ephemeral_Sand_Rivers_Sahel_GEE.

All the raw datasets used in this study and visualized through the platform are available for download at: https://doi.org/10.5281/zenodo.17398126 (Belemtougri et al., 2025b).

References

Akin-Oriola, G., Anetekhai, M., , et al.Oriola, A., 2006. Algal blooms in Nigerian waters: an overview. Afr. J. Mar. Sci. 28 (2), 219–224. https://doi.org/10.2989/18142320609504151.

Beck, H.E., Zimmermann, N.E., McVicar, T.R., Vergopolan, N., Berg, A., , et al.Wood, E.F., 2018. Present and future Köppen-Geiger climate classification maps at 1-km resolution. Sci. Data 5 (1), 180214. https://doi.org/10.1038/sdata.2018.214.

Belemtougri, A.P., Ducharne, A., , et al.Karambiri, H., 2021a. Improvement of river network representation in Africa: application of an approach based on digital elevation data and environmental characteristics. Proceed. Int. Assoc. Hydrol. Sci. 384, 19–23. https://doi.org/10.5194/piahs-384-19-2021.

Belemtougri, A.P., Ducharne, A., Tazen, F., Oudin, L., , et al.Karambiri, H., 2021b. Understanding key factors controlling the duration of river flow intermittency: case of Burkina Faso in West Africa. J. Hydrol.: Reg. Stud. 37, 100908. https://doi.org/10.1016/j.ejrh.2021.100908.

Belemtougri, A.P., Ducharne, A., Tazen, F., Oudin, L., , et al.Karambiri, H., 2025a. Spatial Patterns and Controlling Factors of River Flow Intermittency in Africa. Submitted to Water Resources Research. https://doi.org/10.5281/zenodo.16218062.

Belemtougri, A., Yonaba, R., Michailovsky, C., Stigter, T., Mounirou, L.A., van der Zaag, P., 2025b. Dataset for "Where rivers sleep: mapping ephemeral sand rivers in the West African Sahel". Zenodo. https://doi.org/10.5281/zenodo.17398126 [Data set].

Belgiu, M., Drăguţ, L., 2016. Random forest in remote sensing: a review of applications and future directions. ISPRS J. Photogrammetry Remote Sens. 114, 24–31. https://doi.org/10.1016/j.isprsjprs.2016.01.011.

Benjaminsen, T.A., , et al.Svarstad, H., 2021. Climate Change, Scarcity and Conflicts in the Sahel. Dans T. A. Benjaminsen Et H. Svarstad, Political Ecology. Springer International Publishing, pp. 183–205. https://doi.org/10.1007/978-3-030-56036-2_8.

Biasutti, M., 2019. Rainfall trends in the African Sahel: characteristics, processes, and causes. Wiley Interdiscip. Rev.: Clim. Change 10 (4), e591. https://doi.org/10.1002/wcc.591.

Biau, G., Scornet, E., 2016. A random forest guided tour. TEST 25 (2), 197–227. https://doi.org/10.1007/s11749-016-0481-7.
Boschetto, R.G., Mohamed, R.M., , et al.Arrigotti, J., 2010. Vulnerability to desertification in a sub-saharan region: a first local assessment in five villages of southern region of Malawi. Ital. J. Agron. 5 (s3), 91–102. https://doi.org/10.4081/ija.2010.s3.91.
Boulesteix, A., Janitza, S., Kruppa, J., et König, I.R., 2012. Overview of random forest methodology and practical guidance with emphasis on computational biology and bioinformatics. Wiley Interdiscip. Rev.: Data Min. Knowl. Discov. 2 (6), 493–507. https://doi.org/10.1002/widm.1072.
Breiman, L., 2001. Random forests. Mach. Learn. 45 (1), 5–32. https://doi.org/10.1023/A:1010933404324.
Bremer, K., 2022. AN EARTH OBSERVATION–BASED IDENTIFICATION METHOD FOR EPHEMERAL RIVERS IN SUB-SAHARAN AFRICA.
Castellazzi, P., Gao, S., Pritchard, J., Ponce-Reyes, R., Stratford, D., , et al.Crosbie, R., 2024. Detecting springs and groundwater-dependent vegetation in data-scarce regions of Australia combining citizen science, GRACE, and optical/radar imagery. Rem. Sens. Environ. 313, 114345. https://doi.org/10.1016/j.rse.2024.114345.
Castelli, G., Bresci, E., Castelli, F., Hagos, E.Y., , et al.Mehari, A., 2018. A participatory design approach for modernization of spate irrigation systems. Agric. Water Manag. 210, 286–295. https://doi.org/10.1016/j.agwat.2018.08.030.
Codjia, A.K.D., Akpoti, K., Dembélé, M., Yonaba, R., Fowe, T., Sankande, S., Koissi, M.G.D.-G., , et al.Zwart, S.J., 2025. Estimating water levels in reservoirs using Sentinel-2 derived time series of surface water areas: a case study of 20 reservoirs in Burkina Faso. Int. J. Appl. Earth Obs. Geoinf. 139, 104523. https://doi.org/10.1016/j.jag.2025.104523.
Costigan, K.H., Kennard, M.J., Leigh, C., Sauquet, E., Datry, T., , et al.Boulton, A.J., 2017. Flow regimes in intermittent Rivers and ephemeral streams. Dans *Intermittent Rivers and Ephemeral Streams*. Elsevier, pp. 51–78. https://doi.org/10.1016/B978-0-12-803835-2.00003-6.
Cunningham, S.C., Thomson, J.R., Mac Nally, R., Read, J., et Baker, P.J., 2011. Groundwater change forecasts widespread forest dieback across an extensive floodplain system: groundwater change forecasts forest dieback. Freshw. Biol. 56 (8), 1494–1508. https://doi.org/10.1111/j.1365-2427.2011.02585.x.
Cutler, D.R., Edwards Jr, T.C., Beard, K.H., Cutler, A., Hess, K.T., Gibson, J., , et al.Lawler, J.J., 2007. Random forests for classification in ecology. Ecology 88 (11), 2783–2792. https://doi.org/10.1890/07-0539.1.
Dembélé, M., Zwart, S.J., 2016. Evaluation and comparison of satellite-based rainfall products in Burkina Faso, West Africa. Int. J. Rem. Sens. 37 (17), 3995–4014. https://doi.org/10.1080/01431161.2016.1207258.
Döll, P., Abbasi, M., Messager, M.L., Trautmann, T., Lehner, B., Lamouroux, N., 2024. Streamflow intermittence in Europe : estimating high-resolution monthly time series by downscaling of simulated runoff and random forest modeling. Water Resour. Res. 60 (8). https://doi.org/10.1029/2023WR036900 e2023WR036900.
Donat, M.G., Lowry, A.L., Alexander, L.V., O'Gorman, P.A., , et al.Maher, N., 2016. More extreme precipitation in the world's dry and wet regions. Nat. Clim. Change 6 (5), 508–513. https://doi.org/10.1038/nclimate2941.
Drusch, M., Del Bello, U., Carlier, S., Colin, O., Fernandez, V., Gascon, F., Hoersch, B., Isola, C., Laberinti, P., Martimort, P., Meygret, A., Spoto, F., Sy, O., Marchese, F., , et al.Bargellini, P., 2012. Sentinel-2: esa's optical high-resolution mission for GMES operational services. Rem. Sens. Environ. 120, 25–36. https://doi.org/10.1016/j.rse.2011.11.026.
Duker, A., Cambaza, C., Saveca, P., Ponguane, S., Mawoyo, T.A., Hulshof, M., Nkomo, L., Hussey, S., Van Den Pol, B., Vuik, R., Stigter, T., et Van Der Zaag, P., 2020. Using nature-based water storage for smallholder irrigated agriculture in African drylands: lessons from frugal innovation pilots in Mozambique and Zimbabwe. Environ. Sci. Pol. 107, 1–6. https://doi.org/10.1016/j.envsci.2020.02.010.
Eisma, J.A., Merwade, V., 2021. A data-driven approach to assessing the impact of water harvesting structures on regional water storage in East Africa. J. Hydroinform. 23 (2), 352–367. https://doi.org/10.2166/hydro.2021.115.
Fovet, O., Belemtougri, A., Boithias, L., Braud, I., Charlier, J., Cottet, M., Daudin, K., Dramais, G., Ducharne, A., Folton, N., Grippa, M., Hector, B., Kuppel, S., Le Coz, J., Legal, L., Martin, P., Moatar, F., Molénat, J., Probst, A., et al., 2021. Intermittent rivers and ephemeral streams: perspectives for critical zone science and research on socio-ecosystems. Wiley Interdiscip. Rev.: Water 8 (4), e1523. https://doi.org/10.1002/wat2.1523.
Fowé, T., Yonaba, R., Mounirou, L.A., Ouédraogo, E., Ibrahim, B., Niang, D., Karambiri, H., , et al.Yacouba, H., 2023. From meteorological to hydrological drought: a case study using standardized indices in the Nakanbe River basin, Burkina Faso. Nat. Hazards 119 (3), 1941–1965. https://doi.org/10.1007/s11069-023-06194-5.
Froidurot, S., Diedhiou, A., 2017. Characteristics of wet and dry spells in the West African monsoon system: characteristics of wet and dry spells in West Africa. Atmos. Sci. Lett. 18 (3), 125–131. https://doi.org/10.1002/asl.734.
Funk, C., Peterson, P., Landsfeld, M., Pedreros, D., Verdin, J., Shukla, S., Husak, G., Rowland, J., Harrison, L., , et al.Hoell, A., 2015. The climate hazards infrared precipitation with stations—a new environmental record for monitoring extremes. Sci. Data 2 (1), 1–21. https://doi.org/10.1038/sdata.2015.66.
Giannini, A., Biasutti, M., , et al.Verstraete, M.M., 2008. A climate model-based review of drought in the Sahel: desertification, the re-greening and climate change. Global Planet. Change 64 (3–4), 119–128. https://doi.org/10.1016/j.gloplacha.2008.05.004.
Girard, F., Kergoat, L., Nikiema, H., Wubda, M., Yonaba, R., Fowé, T., Touré, A.A., Mainassara, I., De Fleury, M., , et al.Grippa, M., 2025. Comparison of methods to derive the height-area relationship of shallow Lakes in West Africa using remote sensing. Water Resour. Res. 61 (2). https://doi.org/10.1029/2024WR037411 e2024WR037411.
Goodrich, D.C., Kepner, W.G., Levick, L.R., , et al.Wigington, P.J., 2018. Southwestern intermittent and ephemeral stream connectivity. JAWRA J. Am. Water Resour. Assoc. 54 (2), 400–422. https://doi.org/10.1111/1752-1688.12636.
Gorelick, N., Hancher, M., Dixon, M., Ilyushchenko, S., Thau, D., et Moore, R., 2017. Google Earth engine: planetary-Scale geospatial analysis for everyone. Rem. Sens. Environ. 202, 18–27. https://doi.org/10.1016/j.rse.2017.06.031.
Herbert, R., Barker, J.A., Davies, J., , et al.Katai, O.T., 1997. Exploiting ground water from sand rivers in Botswana using collector wells. Dans *Hydrogeology*. CRC Press, pp. 235–257. https://www.taylorfrancis.com/chapters/edit/10.1201/9781003079521-27/exploiting-ground-water-sand-rivers-botswana-using-collector-wells-herbert-barker-davies-katai.
IGB(Institut Géographique du Burkina), 2012. In: BNDT (Base Nationale des Données Topographiques). http://www.igb.bf/?page_id=85.
IGM(Institut Géographique du Mali), 2016. Document De Spécifications Externes De Contenu De La Base Hydrographoque.
Jalloh, A., Nelson, G.C., Thomas, T.S., Zougmoré, R.B., , et al.Roy-Macauley, H., 2013. Chapter 4 in West African agriculture and climate change: a comprehensive analysis. IFPRI Res. Monograph. Washington, D.C. Intl Food Policy Res. Inst. https://doi.org/10.2499/9780896292048.
JAXA, 2019. ALOS global Digital Surface Model (DSM) ALOS world 3D-30m (AW3D30) version 2.2 product description. https://www.eorc.jaxa.jp/ALOS/en/aw3d30/aw3d30v22_product_e.pdf.
Kaboré, M.P.J., Lawane, A., Yonaba, R., Biaou, A.C., Nadjibou, A., , et al.Pantet, A., 2024. Why do small earth dams deteriorate: insights from physical investigations in the West African Sahel. Resources 13 (6), 71. https://doi.org/10.3390/resources13060071.
Kafando, M.B., Koïta, M., Coz, M.L., Yonaba, O.R., Fowe, T., Zouré, C.O., Faye, M.D., , et al.Leye, B., 2021. Use of Multidisciplinary Approaches for Groundwater Recharge Mechanism Characterization in Basement Aquifers: Case of Sanon Experimental Catchment in Burkina Faso, vol. 22. https://doi.org/10.3390/w13223216.
Kafando, M.B., Koïta, M., Zouré, C.O., Yonaba, R., , et al.Niang, D., 2022. Quantification of soil deep drainage and aquifer recharge dynamics according to land use and land cover in the basement zone of Burkina Faso in West Africa. Sustainability 14 (22), 14687. https://doi.org/10.3390/su142214687.
Kardjadj, M., 2019. The African Sahel Region: an introduction. Dans M. Kardjadj, A. Diallo Et R. Lancelot (Dir.), Transboundary Animal Diseases in Sahelian Africa and Connected Regions. Springer International Publishing, pp. 3–9. https://doi.org/10.1007/978-3-030-25385-1_1.
Lazurko, A., Lautze, J., Hussey, S., Muzarabani, C., Ngwenya, N., , et al.Ebrahim, G., 2024. Assessing sand dams for contributions to local water security and drought resilience in the semi-arid eastern Shashe catchment, Zimbabwe. Reg. Environ. Change 24 (2), 36. https://doi.org/10.1007/s10113-024-02201-y.
Le Houérou, H.N., 2009. Bioclimatology and Biogeography of Africa. Springer Berlin Heidelberg. https://doi.org/10.1007/978-3-540-85192-9.
Lèye, B., Zouré, C.O., Yonaba, R., , et al.Karambiri, H., 2021. Water resources in the Sahel and adaptation of agriculture to climate change: Burkina Faso. Dans S. Diop, P. Scheren Et A. Niang (Dir.), Climate Change and Water Resources in Africa. Springer International Publishing, pp. 309–331. https://doi.org/10.1007/978-3-030-61225-2_14.

Li, Z., Weng, Q., Zhou, Y., Dou, P., et Ding, X., 2024. Learning spectral-indices-fused deep models for time-series land use and land cover mapping in cloud-prone areas: the case of Pearl River Delta. Rem. Sens. Environ. 308, 114190. https://doi.org/10.1016/j.rse.2024.114190.
Lindsay, J.B., 2016. The practice of DEM stream burning revisited. Earth Surf. Process. Landf. 41 (5), 658–668. https://doi.org/10.1002/esp.3888.
Linke, S., Lehner, B., Ouellet Dallaire, C., Ariwi, J., Grill, G., Anand, M., Beames, P., Burchard-Levine, V., Maxwell, S., Moidu, H., Tan, F., , et al.Thieme, M., 2019. Global hydro-environmental sub-basin and river reach characteristics at high spatial resolution. Sci. Data 6 (1), 283. https://doi.org/10.1038/s41597-019-0300-6.
Love, D., Van Der Zaag, P., Uhlenbrook, S., et Owen, R.J.S., 2011. A water balance modelling approach to optimising the use of water resources in ephemeral sand Rivers. River Res. Appl. 27 (7), 908–925. https://doi.org/10.1002/rra.1408.
Mansell, M.G., Hussey, S.W., 2005. An investigation of flows and losses within the alluvial sands of ephemeral Rivers in Zimbabwe. J. Hydrol. 314 (1–4), 192–203. https://doi.org/10.1016/j.jhydrol.2005.03.015.
Marešová, J., Bašta, P., Gdulová, K., Barták, V., Kozhoridze, G., Šmída, J., Markonis, Y., Rocchini, D., Prošek, J., Pracná, P., et Moudrý, V., 2024. Choosing the optimal global digital elevation model for stream network delineation: beyond vertical accuracy. Earth Space Sci. 11 (12). https://doi.org/10.1029/2024EA003743 e2024EA003743.
Marzouki, A., Dridri, A., 2022. Normalized difference enhanced sand index for desert sand dunes detection using Sentinel-2 and landsat 8 OLI data, application to the north of Figuig, Morocco. J. Arid Environ. 198, 104693. https://doi.org/10.1016/j.jaridenv.2021.104693.
Messager, M.L., Lehner, B., Cockburn, C., Lamouroux, N., Pella, H., Snelder, T., Tockner, K., Trautmann, T., Watt, C., , et al.Datry, T., 2021. Global prevalence of non-perennial rivers and streams. Nature 594 (7863), 391–397. https://doi.org/10.1038/s41586-021-03565-5.
Morin, E., Grodek, T., Dahan, O., Benito, G., Kulls, C., Jacoby, Y., Langenhove, G.V., Seely, M., et Enzel, Y., 2009. Flood routing and alluvial aquifer recharge along the ephemeral arid Kuiseb River, Namibia. J. Hydrol. 368 (1–4), 262–275. https://doi.org/10.1016/j.jhydrol.2009.02.015.
Mortimore, M., Anderson, S., Cotula, L., Davies, J., Faccer, K., Hesse, C., Morton, J., Nyangena, W., Skinner, J., et Wolfangel, C., 2009. Dryland Opportunies: a New Paradigm for People, Ecosystems and Development. International Union for Conservation of Nature (IUCN). https://www.iied.org/sites/default/files/pdfs/migrate/G02572.pdf.
Mpala, S.C., Gagnon, A.S., Mansell, M.G., , et al.Hussey, S.W., 2016. The hydrology of sand rivers in Zimbabwe and the use of remote sensing to assess their level of saturation. Phys. Chem. Earth, Parts A/B/C 93, 24–36. https://doi.org/10.1016/j.pce.2016.03.004.
Niang, I., Ruppel, O., Abdrabo, M., Ama, E., Lennard, C., Padgham, J., , et al.Urquhart, P., 2014. Chapter 22 Africa. In: Climate Change 2014: Impacts, Adaptation, and Vulnerability. Part B: Regional Aspects. Contribution of Working Group II to the Fifth Assessment Report of the Intergovernmental Panel on Climate Change, pp. 1199–1265. https://doi.org/10.1017/CBO9781107415386.002.
Nicholson, S.E., 2013. The West African Sahel: a review of recent studies on the rainfall regime and its interannual variability. ISRN Meteorol. 2013, 1–32. https://doi.org/10.1155/2013/453521.
Nkiaka, E., Bryant, R.G., Dembélé, M., Yonaba, R., Priscilla, A.I., , et al.Karambiri, H., 2024. Quantifying the effects of climate and environmental changes on evapotranspiration variability in the Sahel. J. Hydrol. 642, 131874. https://doi.org/10.1016/j.jhydrol.2024.131874.
Nori, M., Davies, J., 2007. Change of wind or wind of change. *Climate Change, Adaptation and Pastoralism, WISP*, IUCN: Nairobi. https://www.academia.edu/download/34826987/WISP_change_of_wind.pdf.
Nygren, B.L., O'Reilly, C.E., Rajasingham, A., Omore, R., Ombok, M., Awuor, A.O., Jaron, P., Moke, F., Vulule, J., , et al.Laserson, K., 2016. The relationship between distance to water source and moderate-to-severe diarrhea in the global enterics multi-center study in Kenya, 2008–2011. Am. J. Trop. Med. Hyg. 94 (5), 1143. https://doi.org/10.4269/ajtmh.15-0393.
O'Gorman, P.A., 2015. Precipitation extremes under climate change. Curr. Clim. Change Rep. 1 (2), 49–59. https://doi.org/10.1007/s40641-015-0009-3.
Pan, X., Zhu, X., Yang, Y., Cao, C., Zhang, X., et Shan, L., 2018. Applicability of downscaling land surface temperature by using normalized difference sand index. Sci. Rep. 8 (1), 9530. https://doi.org/10.1038/s41598-018-27905-0.
Panthou, G., Vischel, T., , et al.Lebel, T., 2014. Recent trends in the regime of extreme rainfall in the central Sahel. Int. J. Climatol. 34 (15), 3998–4006. https://doi.org/10.1002/joc.3984.
Peel, M.C., Finlayson, B.L., , et al.McMahon, T.A., 2007. Updated world map of the Köppen-Geiger climate classification. Hydrol. Earth Syst. Sci. 11 (5), 1633–1644. https://doi.org/10.5194/hess-11-1633-2007.
PNA, B., 2015. Plan national D'ADAPTATION aux changements CLIMATIQUES (PNA) du Burkina Faso. Ministère de l'environnement et du cadre du vie, Burkina Faso. https://www4.unfccc.int/sites/NAPC/Documents/Parties/PNA_Version_version%20francaise%20finale%20BF.pdf.
Prasad, P., Duker, A., de Fraiture, C., et van der Zaag, P., 2023. Irrigation development under uncertainty: a call for adaptive investment pathways. Environ. Sci. Pol. 140, 104–110. https://doi.org/10.1016/j.envsci.2022.11.017.
Prasad, P., Duker, A., Velasquez, D.Z., Chauruka, M., Karimba, B.M., de Fraiture, C., Manzungu, E., et van der Zaag, P., 2024. From few large to many small investments: lessons for adaptive irrigation development in an uncertain world. Front. Water 6, 1296262. https://doi.org/10.3389/frwa.2024.1296262.
Rau, G.C., Halloran, L.J.S., Cuthbert, M.O., Andersen, M.S., Acworth, R.I., , et al.Tellam, J.H., 2017. Characterising the dynamics of surface water-groundwater interactions in intermittent and ephemeral streams using streambed thermal signatures. Adv. Water Resour. 107, 354–369. https://doi.org/10.1016/j.advwatres.2017.07.005.
Raynaut, C., 2001. Societies and nature in the Sahel: ecological diversity and social dynamics. Glob. Environ. Change 11 (1), 9–18. https://doi.org/10.1016/S0959-3780(00)00041-8.
Rossi, V., Krtalić, A., , et al.Buzjak, N., 2025. Land cover mapping in mountainous Croatia using Sentinel-2A satellite imagery. Environ. Earth Sci. 84 (17), 499. https://doi.org/10.1007/s12665-025-12510-y.
Ryan, C., Elsner, P., 2016. The potential for sand dams to increase the adaptive capacity of East African drylands to climate change. Reg. Environ. Change 16 (7), 2087–2096. https://doi.org/10.1007/s10113-016-0938-y.
Sanogo, M., Yonaba, R., Lawane, A., Zorom, M., Tassembédo, F., Ali Sahad, H., et Bazié, I., 2024. Do runoff water harvesting ponds affect farmers cropping choices? Insights from smallholders in the West African Sahel. Sustainability 16 (18), 8000. https://doi.org/10.3390/su16188000.
Saveca, P.S.L., Abi, A., Stigter, T.Y., Lukas, E., , et al.Fourie, F., 2022a. Assessing groundwater dynamics and hydrological processes in the sand river deposits of the Limpopo River, Mozambique. Front. Water 3, 731642. https://doi.org/10.3389/frwa.2021.731642.
Saveca, P.S.L., Abi, A., Stigter, T.Y., Lukas, E., , et al.Fourie, F., 2022b. Assessing groundwater dynamics and hydrological processes in the Sand River deposits of the Limpopo River, Mozambique. Front. Water 3, 731642. https://doi.org/10.3389/frwa.2021.731642.
Schilling, O.S., Cook, P.G., Grierson, P.F., Dogramaci, S., et Simmons, C.T., 2021. Controls on interactions between surface water, groundwater, and riverine vegetation along intermittent Rivers and ephemeral streams in arid regions. Water Resour. Res. 57 (2). https://doi.org/10.1029/2020WR028429 e2020WR028429.
Secu, C.V., Stoleriu, C.C., Lesenciuc, C.D., , et al.Ursu, A., 2022. Normalized sand index for identification of bare sand areas in temperate climates using landsat images, application to the south of Romania. Remote Sens. 14 (15), 3802. https://doi.org/10.3390/rs14153802.
Shakhane, T., Fourie, F.D., et Du Preez, P.J., 2017. Mapping riparian vegetation and charactersing its groundwater dependency at the modder river government water scheme. Groundw. Sustain. Dev. 5, 216–228. https://doi.org/10.1016/j.gsd.2017.07.003.
Shanafield, M., Cook, P.G., 2014. Transmission losses, infiltration and groundwater recharge through ephemeral and intermittent streambeds: a review of applied methods. J. Hydrol. 511, 518–529. https://doi.org/10.1016/j.jhydrol.2014.01.068.
Sultan, B., Gaetani, M., 2016. Agriculture in West Africa in the twenty-first century: climate change and impacts scenarios, and potential for adaptation. Front. Plant Sci. 7, 1262. https://doi.org/10.1023/A:1026014311149.
Svubure, O., Gumbo, T., Soropa, G., Rusere, F., Ndeketeya, A., , et al.Moyo, D., 2011. Evaluation of the sand abstraction systems for rural water supply: the case of lupane district, Zimbabwe. Int. J. Eng. Sci. Technol. 3 (1). https://www.researchgate.net/publication/50392227_Evaluation_of_the_Sand_Abstraction_Systems_for_Rural_Water_Supply_the_case_of_Lupane_District_Zimbabwe.

Thirumalraj, A., Anusuya, V.S., , et al.Manjunatha, B., 2023. Detection of Ephemeral Sand River Flow Using Hybrid Sandpiper Optimization-Based CNN Model: Dans A. Kumar, A. L. Srivastav, A. K. Dubey, V. Dutt et N. Vyas (dir.). Advances in Civil and Industrial Engineering. IGI Global, pp. 195–214. https://doi.org/10.4018/979-8-3693-1194-3.ch010.

Todzo, S., Bichet, A., , et al.Diedhiou, A., 2020. Intensification of the hydrological cycle expected in West Africa over the 21st century. Earth Syst. Dyn. 11 (1), 319–328. https://doi.org/10.5194/esd-11-319-2020.

Tolan, J., Yang, H.-I., Nosarzewski, B., Couairon, G., Vo, H.V., Brandt, J., Spore, J., Majumdar, S., Haziza, D., , et al.Vamaraju, J., 2024. Very high resolution canopy height maps from RGB imagery using self-supervised vision transformer and convolutional decoder trained on aerial lidar. Rem. Sens. Environ. 300, 113888. https://doi.org/10.1016/j.rse.2023.113888.

Tyralis, H., Papacharalampous, G., , et al.Langousis, A., 2019. A brief review of random forests for water scientists and practitioners and their recent history in water resources. Water 11 (5), 910. https://doi.org/10.3390/w11050910.

United Nations. World population prospects 2022. UN DESA. https://www.un.org/development/desa/pd/sites/www.un.org.development.desa.pd/files/wpp2022_summary_of_results.pdf.

Villeneuve, S., Cook, P.G., Shanafield, M., Wood, C., et White, N., 2015. Groundwater recharge via infiltration through an ephemeral riverbed, central Australia. J. Arid Environ. 117, 47–58. https://doi.org/10.1016/j.jaridenv.2015.02.009.

Vio, D., de Souza, J.O.P., Motta, G.H.M.B., , et al.de Souza, L.C., 2025. Machine learning on alluvial deposit identification in dryland area. Revista Contexto Geográfico 10 (24), 138–182. https://doi.org/10.28998/contegeo.10i.24.18434.

Walker, D., Smigaj, M., , et al.Jovanovic, N., 2019. Ephemeral sand river flow detection using satellite optical remote sensing. J. Arid Environ. 168, 17–25. https://doi.org/10.1016/j.jaridenv.2019.05.006.

Wang, T., Wu, Z., Wang, P., Wu, T., Zhang, Y., Yin, J., Yu, J., Wang, H., Guan, X., , et al.Xu, H., 2023. Plant-groundwater interactions in drylands: a review of current research and future perspectives. Agric. For. Meteorol. 341, 109636. https://doi.org/10.1016/j.agrformet.2023.109636.

Wekesa, S.S., Stigter, T.Y., Olang, L.O., Oloo, F., Fouchy, K., , et al.McClain, M.E., 2020. Water flow behavior and storage potential of the semi-arid ephemeral River system in the Mara Basin of Kenya. Front. Environ. Sci. 8, 95. https://doi.org/10.3389/fenvs.2020.00095.

Wilson, E.B., 1927. Probable inference, the law of succession, and statistical inference. J. Am. Stat. Assoc. 22 (158), 209–212. https://doi.org/10.1080/01621459.1927.10502953.

WorldPop, 2020. Global high-resolution Population : Populations Counts, Constrained Individual Countries 2020 UN Adjusted - 100 M Resolution. University of Southampton). https://hub.worldpop.org/geodata/listing?id=79.

Wortmann, M., Slater, L., Hawker, L., Liu, Y., Neal, J., Zhang, B., Schwenk, J., Allen, G., Ashworth, P., Boothroyd, R., Cloke, H., Delorme, P., Gebrechorkos, S.H., Griffith, H., Leyland, J., McLelland, S., Nicholas, A.P., Sambrook-Smith, G., Vahidi, E., et al., 2025. Global River topology (GRIT): a bifurcating River hydrography. Water Resour. Res. 61 (5). https://doi.org/10.1029/2024WR038308 e2024WR038308.

Xu, H., 2006. Modification of normalised difference water index (NDWI) to enhance open water features in remotely sensed imagery. Int. J. Rem. Sens. 27 (14), 3025–3033. https://doi.org/10.1080/01431160600589179.

Yamazaki, D., Ikeshima, D., Sosa, J., Bates, P.D., Allen, G.H., , et al.Pavelsky, T.M., 2019. MERIT hydro: a high-resolution global hydrography map based on latest topography dataset. Water Resour. Res. 55 (6), 5053–5073. https://doi.org/10.1029/2019WR024873.

Yamazaki, D., Ikeshima, D., Tawatari, R., Yamaguchi, T., O'Loughlin, F., Neal, J.C., Sampson, C.C., Kanae, S., , et al.Bates, P.D., 2017. A high-accuracy map of global terrain elevations: accurate global terrain elevation map. Geophys. Res. Lett. 44 (11), 5844–5853. https://doi.org/10.1002/2017GL072874.

Yonaba, R., Belemtougri, A., Fowé, T., Mounirou, L.A., Nkiaka, E., Dembélé, M., Komlavi, A., Coly, S.M., Koïta, M., , et al.Karambiri, H., 2024. Rainfall estimation in the West African Sahel: comparison and cross-validation of top-down *vs.* bottom-up precipitation products in Burkina Faso. Geocarto Int. 39 (1), 2391956. https://doi.org/10.1080/10106049.2024.2391956.

Yonaba, R., Kiema, A., Tazen, F., Belemtougri, A., Cissé, M., Mounirou, L.A., Bodian, A., Koïta, M., , et al.Karambiri, H., 2025. Accuracy and interpretability of machine learning-based approaches for daily ETo estimation under semi-arid climate in the West African Sahel. Earth Sci. Inform. 18 (1), 87. https://doi.org/10.1007/s12145-024-01591-1.

Yonaba, R., Koïta, M., Mounirou, L., Tazen, F., Queloz, P., Biaou, A., Niang, D., Zouré, C., Karambiri, H., , et al.Yacouba, H., 2021. Spatial and transient modelling of land use/land cover (LULC) dynamics in a Sahelian landscape under semi-arid climate in northern Burkina Faso. Land Use Policy 103, 105305. https://doi.org/10.1016/j.landusepol.2021.105305.